

Mathematical Evolution Models in the Life Sciences.

Prof. Dr. W. Govaerts

1 February 2010

# Contents

<b>1</b>	<b>Modelling a neuron</b>	<b>3</b>
1.1	Modeling a neuron. . . . .	4
1.1.1	Molecules, atoms, electrons and ions. . . . .	4
1.1.2	The basic gating mechanism. . . . .	6
1.1.3	The mathematical solution of the gating equation for fixed rate constants. . . . .	7
1.1.4	The Nernst potential. . . . .	7
1.1.5	The membrane model. . . . .	9
1.1.6	The voltage clamp. . . . .	10
1.2	The fast Morris-Lecar model for the barnacle muscle fiber. . . . .	12
1.2.1	Description of the model. . . . .	12
1.3	Exercises . . . . .	13
<b>2</b>	<b>Computational study of the Morris-Lecar equations</b>	<b>17</b>
2.1	Simulation study of the fast Morris-Lecar equations. . . . .	17
2.1.1	Stable and unstable equilibria and their continuation . . . . .	20
2.1.2	Continuation of periodic orbits . . . . .	21
2.2	Two-parameter study of the fast Morris-Lecar model. . . . .	21
2.2.1	Bogdanov-Takens points. . . . .	21
2.2.2	Generalized Hopf points. . . . .	26
2.3	Excitability in the fast Morris-Lecar model. . . . .	29
2.3.1	Type I excitability. . . . .	29
2.3.2	Type II excitability. . . . .	29
2.4	The slow-fast Morris-Lecar model for the barnacle muscle fiber. . . . .	35
2.4.1	Description of the slow-fast model. . . . .	35
2.4.2	Bursting in the slow-fast model. . . . .	35
2.5	Exercises . . . . .	38
<b>3</b>	<b>A full two-parameter picture</b>	<b>40</b>
3.1	The global picture. . . . .	40
3.1.1	Equilibria . . . . .	40
3.1.2	Limit cycles . . . . .	40
3.2	Exercises . . . . .	46
<b>4</b>	<b>Cell cycle controls</b>	<b>48</b>
4.1	The basic mechanisms . . . . .	48
4.1.1	The phases of the cell cycle . . . . .	48

4.1.2	The regulatory mechanism . . . . .	49
4.1.3	Example: the budding yeast equations. . . . .	52
4.2	The toy model of Tyson and Novak . . . . .	55
4.2.1	The model with constant Cdh1/APC activator . . . . .	55
4.2.2	A dynamic Cdh1/APC activator . . . . .	57
4.3	Orbits homoclinic to saddle-node . . . . .	60
4.4	The cell cycle as a slow-fast system: insensitivity to the initial values . . . . .	60
4.5	The cell cycle as a boundary value problem . . . . .	63
4.6	Exercises . . . . .	64

# Chapter 1

## Modelling a neuron

From the early days of the study of electricity it was known that muscle activity of animals is related to electricity. Credit for the discovery of this is due to Luigi Galvani (1737-1798), a medical doctor and anatomist. In 1771, he discovered that the muscles of dead frogs twitched when struck by a scalpel that had picked up some electric charge.

Galvani believed that what he called animal electricity came from the muscle. He regarded their activation as being generated by an electrical fluid that is carried to the muscles by the nerves.

Galvani's associate and opponent, the physicist Alessandro Volta (1745-1825), in opposition, reasoned that the animal electricity was a physical phenomenon, a metallic electricity.

Volta's intuition was correct. While all life is indeed electrical, specifically all living things are made of cells and every cell has a cell potential, biological electricity has the same chemical underpinnings as the current between electrochemical cells, and thus can be recapitulated in a way outside the body. Thus, owing to an argument between the two in regard to the source or cause of the electricity, Volta built the first battery in order to specifically disprove his associate's theory. Volta's pile became known therefore as a voltaic pile.

Volta objected to Galvani's conclusions about "animal electric fluid", but the two scientists disagreed respectfully and Volta coined the term "galvanism" for a direct current of electricity produced by chemical action.

A neuron (in an animal or human brain) is a modified muscle cell whose main task is communication, not movement of body parts. So, in a sense, thinking is a form of moving. It has been certified experimentally that the same parts of the brain are activated whether one thinks about moving a leg or actually moving it.

A typical neuron possesses a cell body (often called soma), dendrites, and an axon. Dendrites are filaments of protoplasm that extrude from the cell body, often extending for hundreds of microns and branching multiple times, giving rise to a complex "dendritic tree". An axon is a special protoplasmic filament that arises from the cell body at a site called the axon hillock and travels through the body, often for a great distance. The cell body of a neuron frequently gives rise to multiple dendrites, but never to more than one axon, although the axon may branch hundreds of times before it terminates. At the majority of synapses, signals are sent from the axon of one neuron to a dendrite of another.

Unlike many other cells, neurons do not undergo cell division, and usually cannot be replaced after being lost. In most cases they are generated by special types of stem cells.

Neurons are usually small because their task is to be the small, unreliable components of

a big, reliable network (the human brain contains about  $10^{11}$  neurons). Therefore, it is hard to study them experimentally.

However, there are exceptions. Some animals, in particular squids, barnacles, lobsters and some insects have comparatively big neurons and/or axons. The reason for this is presumably that crucial reaction times can be shortened drastically by having long, large neurons; a very short reaction time can save the life of an animal or allow it to catch its prey. While the reaction time of a human is about 0.1s, this can be reduced by a factor 100 in some apparently much simpler creatures.

The first known example of this is the squid giant axon, i.e. the very large (up to 1 mm in diameter; typically around 0.5 mm) axon that controls part of the water jet propulsion system in squid. It was discovered by English zoologist and neurophysiologist John Zachary Young in 1936. Squid use this system primarily for making brief but very fast movements through the water.

Between the tentacles of a squid is a siphon through which water can be rapidly expelled by the fast contractions of the body wall muscles of the animal. This contraction is initiated by action potentials in the giant axon. Action potentials travel faster in a larger axon than a smaller one, and squid have evolved the giant axon to improve the speed of their escape response.

In their Nobel Prize-winning work (Nobel Prize for Physiology or Medicine 1963) uncovering ionic mechanism of action potentials, Alan Hodgkin and Andrew Huxley performed in the early 1950's experiments on the squid giant axon. The large diameter of the axon provided a great experimental advantage for Hodgkin and Huxley as it allowed them to insert voltage clamp electrodes inside the lumen of the axon. This led to the famous Hodgkin - Huxley equation, a system of four nonlinear ODEs.

Later, many other large neurons were discovered and studied experimentally. This includes neurons of the sea hare (in fact, a sort of sea snail), the Jonah crab and the barnacle, an arthropod (hence related to crabs and lobsters) that at first sight resembles a mussel.

We refer to Wikipedia for nice pictures of the animals mentioned above.

In this chapter we discuss the modelling of neurons; we concentrate in particular on the Morris-Lecar neuron. The Morris-Lecar equations grew out of an experimental study of the excitability of the giant muscle fiber of the huge Pacific barnacle, *balanus nubilis* (named by Charles Darwin, who probably meant to call it *balanus nobilis*). The model was published in 1981 [8].

Its complicated dynamical properties will be studied in the next chapters, in particular spiking and bursting. It is generally believed that these phenomena are the basic mechanisms of muscle and neural cells; in particular all information processing in the nervous systems of animals and humans is based on them.

## 1.1 Modeling a neuron.

Most of the present §1.1 is adapted from [3], Chapter 2.

### 1.1.1 Molecules, atoms, electrons and ions.

It is now accepted as a scientific fact that all substances that we see around us consist of molecules. The number of different molecules is huge but they are all formed by combinations of atoms and the number of different atoms is relatively small - one hundred or so. In chemistry

these are called the elements and they are collected in the Periodic Table named after the Russian chemist Mendelejev (1869).

An atom consists of a nucleus and a number of electrons. The nucleus contains neutrons which are electrically neutral and protons which have a basic electrical charge, identical for all protons and by convention said to be positive. This is called the elementary charge  $e$ , cf. Table 1.1. The electrons have the same amount of electrical charge but of an opposite nature, therefore called negative.

An atom is electrically neutral if it surrounded by a number of electrons equal to the number of protons in its nucleus. However, many atoms tend either to lose one or more electrons or to acquire surplus electrons. If this happens then the atom is called an ion. Some ions are very important in electrophysiology, namely:

- Sodium (Na from its Latin name *Natrium*) has atomic number 11, atomic weight 22.99 and valence 1. The latter means that it tends to lose one electron and so form the ion  $\text{Na}^+$ .
- Potassium (K from its Latin name *Kalium*) has atomic number 19, atomic weight 39.102 and valence 1. The latter means that it tends to lose one electron and so form the ion  $\text{K}^+$ .
- Calcium (Ca) has atomic number 20, atomic weight 40.08 and valence 2. The latter means that it tends to lose two electrons and so form the ion  $\text{Ca}^{2+}$ .
- Chlorine (Cl) has atomic number 17, atomic weight 35.45 and valence -1. The latter means that it tends to acquire a surplus electron and so form the ion  $\text{Cl}^-$ .
- Hydrogen (H) has atomic number 1, atomic weight 1.00797 and valence 1. The latter means that it tends to lose one electron and so form the ion  $\text{H}^+$ .
- Oxygen (O) has atomic number 8 and atomic weight 15.9994. It does not normally form ions but has a great capability to bind with other atoms.
- Carbon (C) has atomic number 6 and atomic weight 12. It does not normally form ions but has an even greater capability to bind with other atoms.

We note that the atomic number of an element is the number of protons in the nucleus; therefore it is always a positive integer number. The atomic weight is important in computations that involve concentrations. In the experimental literature the word "concentration" has a precise technical meaning, namely the number of mol of a substance (the solute) that is solved in a liter of solution (solvent+solute). Its unit is the molar, i.e. one mol per liter, cf. Table 1.2. For example, one liter of a sodium ion solution with a concentration of one molar must contain 22.99 grams of sodium since 22.99 is the atomic weight of sodium. The number of ions is then given by Avogadro's number  $N$ , cf. Table 1.1 and their total electrical charge is  $Ne=96485$  Coulomb (cf. Faraday's constant in Table 1.1).

If a molecule consists of several atoms then it has a molecular weight which is obtained by simply adding the atomic weights of the constituting atoms. For example, water ( $\text{H}_2\text{O}$ ) contains two hydrogen atoms (H) with atomic weight 1.00797 and one oxygen atom (O) with atomic weight 15.9994. Therefore the molecular weight of water is  $2 \times 1.00797 + 15.9994 = 18.0153$ .

Definition	Abbreviation	Value
Avogadro's number	N	$6.02214 \times 10^{23}/mol$
Faraday's constant	F	$96485C/mol$
elementary charge	e	$1.60218 \times 10^{-19}C$
gas constant	R	$8.315J/(mol.K)$

Table 1.1: Some important constants. We recall that a mol of a substance is a quantity that contains as many elementary units (atoms or molecules) as there are atoms in 0.012 kg of carbon-12.

Quantity	Symbol	Unit	Symbol
Time	t	Second	s
Current	I	Ampère	A (=C/s)
Charge	Q	Coulomb	C
Capacitance	C	Farad	F (=C/V)
Potential	V	Volt	V (=J/C)
Voltage	U	Volt	V (=J/C)
Resistance	R	Ohm	$\Omega$ (=V/A)
Conductance	g	Siemens	S=mho (=1/ $\Omega$ )
Concentration	$\square$	molar	M (=mol/dm <sup>3</sup> )
Energy	E	Joule	J (=kg.m <sup>2</sup> /s <sup>2</sup> )(=C.V)
Power		Watt	W (=J/s)
Frequency	f	Hertz	Hz (=1/s)

Table 1.2: Important electrical quantities and their units.

### 1.1.2 The basic gating mechanism.

Membranes of excitable cells have so-called channels or gates through which specific ions, in particular  $Na^+$ ,  $K^+$ ,  $Ca^{2+}$ ,  $Cl^-$  can selectively pass. These gates in fact consist of proteins which can be in an open state (O, ions can pass) or a closed state (C, ions cannot pass).

The possible actions consist of switching between the two states. This is usually represented in a simple diagram like (1.1):



The positive real quantities  $k^+$ ,  $k^-$  with dimension  $s^{-1} = Hz$  (Hertz) are called *rate constants* or *proportionality constants*. The meaning of  $k^+$  is as follows. If the concentration of closed states is given by [C], and  $\Delta t$  is a brief time interval, then after time  $\Delta t$ , the part  $k^+[C]\Delta t$  will have opened. Similarly, if the concentration of open states is given by [O], then after time  $\Delta t$ , the part  $k^-[O]\Delta t$  will have closed.

This is a special instance of the principle that is (inappropriately) called the *law of mass action* which states that the rate of a (chemical) process is proportional to the product of the concentrations of the components of the process. At the level of individual molecules, this reduces to a probability but usually one is only interested in the effect on a large number of molecules.

In the present situation only one component is involved. The quantity  $J_+ = k^+[C]$  is called the rate of transition from state C to state O. Similarly,  $J_- = k^-[O]$  is called the rate of transition from state O to state C.

If  $N_C$  and  $N_O$  denote the numbers of channels in the closed state, respectively in the open state, then the quantity  $N = N_C + N_O$  is necessarily fixed. Let us call  $f_C = \frac{N_C}{N}$  the fraction of closed states and  $f_O = \frac{N_O}{N}$  the fraction of open states. Then  $f_O = 1 - f_C$  and we need effectively only an equation for one of  $f_C, f_O$ .

The rate of transition from state O to C is now given by  $j_- = k^- f_O$  and the rate of change from state C to O is given by  $j_+ = k^+(1 - f_O)$ . The difference between these two rates represents the change in  $f_O$  over time:

$$\frac{df_O}{dt} = j_+ - j_- = k^+(1 - f_O) - k^- f_O = -(k^- + k^+)(f_O - \frac{k^+}{k^- + k^+}) \quad (1.2)$$

Now let us denote  $\tau = \frac{1}{k^- + k^+}$  and  $f_\infty = \frac{k^+}{k^- + k^+}$ . Both constants are strictly positive and  $f_\infty$  is in  $]0, 1[$ . We then have

$$\frac{df_O}{dt} = \frac{-(f_O - f_\infty)}{\tau}. \quad (1.3)$$

We note that  $f_O, f_\infty$  are dimensionless and that  $\tau$  has the dimension of time.

### 1.1.3 The mathematical solution of the gating equation for fixed rate constants.

Equation (1.3) holds at a fixed moment in time, even if the rate constants  $k^+, k^-$  (and therefore  $f_\infty$  and  $\tau$ ) are time-dependent. In fact, the rate constants can depend on several external influences, for example temperature, voltage gradient (different electrical potential on the two sides of the membrane), or the presence of chemical substances that block the gates.

We now look at the relatively simple case where there are no such outside influences and  $k^+, k^-$  are constant, so that  $\tau$  and  $f_\infty$  are also constant. In this case, (1.3) is a first order linear differential equation with constant coefficients. The analytical solution to such equations is well known and has the general form:

$$f_O(t) = f_\infty + Ae^{-\frac{t}{\tau}}, \quad (1.4)$$

where  $A$  is an integration constant. The solution is not unique but uniqueness is established as soon as we fix the value of  $f_O(t)$  at any given time  $t$ . For example, if  $f_O(0)$  is known, then we infer from (1.4) that  $f_O(0) = f_\infty + A$ , hence

$$f_O(t) = f_\infty + (f_O(0) - f_\infty)e^{-\frac{t}{\tau}}. \quad (1.5)$$

Obviously, every such solution converges to  $f_\infty$  as  $t$  tends to  $\infty$  and the decay is exponential.

### 1.1.4 The Nernst potential.

Biological fluids such as cytoplasm (intracellular fluid) and extracellular fluid contain many ions. These flow freely in the fluid but cannot always pass through membranes. Typically, membranes contain channels (gates) which are selectively permeable. Therefore, the concentration of an ion inside a cell may be different from the concentration outside the cell. In fact, cells often contain mechanisms that actively maintain concentration differences.

For simplicity, let us consider a case of two monovalent ions  $K^+$  (potassium) and  $Cl^-$  (chlorine). Monovalent means that the electrical charge of a  $K^+$  ion is that of a proton, the charge of a  $Cl^-$  ion is that of an electron. Suppose also that we have two compartments, say  $L$  (left) and  $R$  (right) which are separated by a membrane. (one might think of  $L$  as being the cytoplasm of a cell and of  $R$  as the extracellular fluid).

First suppose that  $L$  has equal concentrations  $[K^+]_L = [Cl^-]_L$  and  $R$  has equal concentrations  $[K^+]_R = [Cl^-]_R$  but the concentrations in  $R$  are higher than the concentrations in  $L$ .

In that case there is no potential difference between the two compartments because the electrical charges in both  $L$  and  $R$  balance.

If we insert a nonselective pore into the cell membrane through which both  $K^+$  and  $Cl^-$  ions can freely pass, then by diffusion the concentrations on both sides will gradually equilibrate. At the end, the potential difference between  $L$  and  $R$  will again be zero.

Suppose, however, that we insert into the membrane an ion-selective pore that allows only the passage of  $K^+$  ions. Since  $[K^+]_R > [K^+]_L$ , the  $K^+$  ions diffuse through the pore from  $R$  to  $L$ . Since the  $Cl^-$  ions cannot pass through the pore, each  $K^+$  ion that passes from  $R$  to  $L$  carries a positive charge that is not counterbalanced by a  $Cl^-$  ion. Because the transfer of these charges establishes an electrical potential gradient,  $K^+$  ions continue to move from high concentration to low concentration until the growing force due to electrical potential difference is balanced by the opposite force generated by the concentration difference.

The *equilibrium potential*, where the electrical and osmotic forces are balanced, is given by the Nernst equation. The Nernst equation is derived from the expression for the change in Gibbs free energy when one mol of an ion of valence  $z$  is moved across a membrane. This change is given by

$$\Delta G = -RT \ln \frac{[ion]_R}{[ion]_L} + (\Delta V)Fz$$

In this expression  $R$  is the gas constant and  $F$  is Faraday's constant (see Table 1.1),  $T$  is the temperature in degrees Kelvin (i.e. temperature in degrees Celsius plus 273.16),  $\Delta V$  is the potential difference across the membrane and  $[ion]_L, [ion]_R$  denote the ion concentrations to the left and to the right of the membrane, respectively.

It is a physical principle that the Gibbs free energy of a system tends to decrease. Therefore the transport of ions through the pore continues as long as  $\Delta G$  is negative. It stops when  $\Delta G = 0$ , i.e. when

$$\Delta V = \frac{RT}{zF} \ln \frac{[ion]_R}{[ion]_L} = \frac{RT \ln 10}{zF} \log_{10} \frac{[ion]_R}{[ion]_L}.$$

To get a rough idea of what this means, we consider body temperature (37 degrees Celsius) and a monovalent ion. For a 10:1 concentration ratio we then get

$$\frac{RT \ln 10}{zF} = (8.315(273.16 + 37) \ln(10)/96485)V = 0.0615V = 61.5mV.$$

Hence a ratio 10:1 in ion concentrations on the two sides of the membrane can compensate for a potential difference of 61.5 mV (milli-Volts). This potential difference is called the Nernst potential. In general, when one starts from any given concentration differences, the ions will move in such a way that the potential difference will gradually evolve to the Nernst potential.

In electrophysiology, the Nernst potential is also called the reversal potential because the departure from that point of zero current flux results in the positive or negative flow of ions.

Ion	Cytoplasmic Concentration (mM)	Extracellular Concentration (mM)
Squid Giant Axon		
K <sup>+</sup>	400	20
Na <sup>+</sup>	50	440
Cl <sup>-</sup>	40	560
Mammalian Neuron		
K <sup>+</sup>	135	3
Na <sup>+</sup>	18	145
Cl <sup>-</sup>	7	120

Table 1.3: Resting ion concentrations. From McCormick [7].

We note that this reversal potential is ion-specific, i.e. each ion has its own reversal potential which is dependent on the ion concentrations on both sides of the membrane (and to a lesser degree on the temperature). In Table 1.3 the resting ion concentrations for the K<sup>+</sup>, Na<sup>+</sup> and Cl<sup>-</sup> ions are given in two neurons. We note that the cell soma contains a large concentration of potassium ions and a low concentration of sodium and chlorine ions, compared to the extracellular fluid.

To get a more precise understanding, suppose we have one liter of extracellular fluid of the squid (the solution). How many grams of potassium ions (the solute) will be dissolved in this amount of fluid? From Table 1.3 we infer that this corresponds to 20 millimolar K<sup>+</sup> ions. Since the atomic weight of potassium is 39.102 (see §1.1.1) this amounts to  $39.102 \times 0.02 = 0.78204$  grams of potassium.

### 1.1.5 The membrane model.

We know from Ohm's law that current flows down a voltage gradient (i.e. from a place with a higher potential to a place with a lower potential) in proportion to the resistance in the circuit. Current is therefore expressed as

$$I = \frac{V}{R} = gV. \quad (1.6)$$

where  $g$  is the inverse of  $R$  and called the conductance. The unit of resistance is the Ohm ( $\Omega$ ) and the unit of conductance is the Siemens ( $S = \frac{1}{\Omega}$ ), cf. Table 1.2.

The conceptual idea behind contemporary electrophysiological models was formulated in the work of K.S. Cole [1], though the fundamental ideas were around some time earlier, e.g. in the pioneering work of A. Hodgkin and A. Huxley [4, 5].

This idea is that a cell membrane can be likened to an electronic circuit in the following sense.

1. A membrane has a phospholipid bilayer which acts as a capacitor, i.e. it accumulates ionic (electrical) charge as the electrical potential across the membrane changes. So it has a capacitance  $C$  and if we denote the potential difference across the membrane (potential on side  $L$  minus potential on side  $R$ ) by  $V$  then an electrical charge of amount  $CV$  is accumulated on the  $L$  side.

2. The ionic permeabilities of the membrane act as resistors in an electric circuit.

3. The electrochemical driving forces for each type of channel are given by the difference between the membrane potential difference and the reversal potential of the corresponding

ion; these driving forces act as batteries driving the ionic circuits.

Now let us work this out in more detail. We take the convention that the potential difference is defined as "inner potential minus outer potential", and that currents are positive if they move from "outside" to "inside". Through the potassium  $K^+$  channel a current passes which by Ohm's law is given by

$$I_K = -g_K(V - V_K), \quad (1.7)$$

where  $g_K$  is the conductance of the  $K^+$  channel; the leading "-" sign is needed because of our conventions about orientation.  $V_K$  is the potassium reversal potential that is determined by the Nernst equation, and  $V - V_K$  is the driving force across the membrane provided by the ionic battery.

We assume that the reversal potential for a given ion is constant; this is equivalent to assuming that there is some restorative mechanism such as ion pumps that can keep pace with electrical activity on a time scale that prevents the ionic battery from running down.

In fact, numerous ions are responsible for the electrical behavior of a cell, and the total current is given by

$$I = \sum_i(-g_i(V - V_i)), \quad (1.8)$$

where the summation is over all ion currents.

In experimental situations the potential difference  $V$  is measured across the membrane and in the process an additional ("applied") current  $I_{app}$  is introduced into the cell. Let us call  $I_{cap} = I_{ion} + I_{app}$  the total (capacitive) current across the cell membrane. From the first assumption of the cell membrane model ( $CV = Q$  where  $Q$  is accumulated charge) we find by derivation that

$$C \frac{dV}{dt} = I_{cap} = I_{ion} + I_{app} = -\sum g_i(V - V_i) + I_{app}, \quad (1.9)$$

where the summation is over all ion channels.

### 1.1.6 The voltage clamp.

In (1.9) the conductances  $g_i$  are not constant in general. Let us denote by  $\bar{g}_i$  the maximum conductance of the  $i$ -th channel, i.e. its conductance when all channels are open. Then we can write  $g_i = \bar{g}_i \cdot f_{iO}$  where  $f_{iO}$  is the fraction of open channels as in §1.1.2. In §1.1.2 we saw that  $f_{iO}$  is time-dependent and its evolution is governed by the equation

$$\frac{df_{iO}}{dt} = \frac{-(f_{iO} - f_{i\infty})}{\tau_i}, \quad (1.10)$$

in which  $f_{i\infty}$ ,  $\tau_i$  are parameters, determined by the rate constants of the ion channels. Moreover, in excitable cells the rate constants of the ion channels are not constant but depend on the potential difference across the membrane. So in fact, (1.10) should be replaced by

$$\frac{df_{iO}}{dt} = \frac{-(f_{iO} - f_{i\infty}(V))}{\tau_i(V)}, \quad (1.11)$$

The voltage clamp is an experimental method designed to measure  $f_{i\infty}(V)$  and  $\tau_i(V)$  directly in a given cell (it is not feasible to measure the rate constants themselves experimentally).

Name (Symbol)	Units	Abbreviation
voltage (V)	$10^{-3}$ volt	mV
time (t)	$10^{-3}$ second	ms
conductance (g)	$10^{-9}$ siemens	nS
capacitance (C)	$10^{-12}$ farad	pF
current (I)	$10^{-12}$ ampere	pA

Table 1.4: Consistent Electrical Units.

In order to measure the voltage across a cell membrane or the current flowing through a membrane, microelectrodes are inserted into cells. These electrodes can be used both to measure current and voltage and to apply external current. The voltage clamp has an electronic feedback device that adjusts the applied current  $I_{app}$  to match and counter the membrane currents such that the membrane voltage is held constant. To see what this accomplishes, consider a membrane with a single gated ionic current. Then (1.9) reduces to

$$C \frac{dV}{dt} = I_{cap} = I_{ion} + I_{app} = -\bar{g}f_O(t)(V - V_{rev}) + I_{app}, \quad (1.12)$$

where  $V_{rev}$  is the reversal potential given by the Nernst equation. If we can hold  $V$  constant, i.e.  $\frac{dV}{dt} = 0$  by applying a current that is equal and opposite to the current flowing through the membrane, then we must have

$$I_{app} = \bar{g}f_O(t)(V - V_{rev})$$

From this type of experiments it is possible to obtain  $V_{rev}$ ,  $\bar{g}$  and  $f_O(t)$  from which eventually  $f_\infty(V)$  and  $\tau(V)$  can be deduced.

To carry out a voltage clamp experiment like this, it is necessary to block all but a single type of current. While this sounds difficult and in fact is not always possible, specific toxins and pharmacological agents have been used successfully.

Also, it is not uncommon in nature. For example, tetrodotoxin (TTX) from the puffer fish selectively blocks voltage gated  $\text{Na}^+$  - channels. Similarly, the toxin of the black mamba (an African snake) selectively blocks the  $\text{K}^+$  - channels. The  $\text{K}^+$ - channels can also be blocked by injecting a large amount of  $\text{K}^+$  ions into the body liquid (normally  $\text{K}^+$  is present in high concentration in the cells and in low concentrations outside). Such injections have been used in the USA to execute criminals convicted of murder [2].

In the future we will drop the overbar in  $\bar{g}$  so that  $g$  will actually denote the maximum conductance which has to be scaled by gating variables of the form  $f_O$ .

To carry out or to simulate a voltage clamp experiment, a consistent set of electrical units must be used. We here discuss the set used in [3]. The standard unit for membrane potentials is millivolts (mV), and the characteristic times for voltage-dependent gates  $\tau$  are in milliseconds. Currents are typically expressed in  $\mu\text{A}/\text{cm}^2$  and capacitances in  $\mu\text{F}/\text{cm}^2$ . For a typical cell of area  $10^{-6}\text{cm}^2$ , this translates to whole-cell current of picoamperes ( $1\text{ pA}=10^{-12}\text{A}$ ) and a whole-cell capacitance of picofarads ( $1\text{ pF}=10^{-12}\text{F}$ ). This set is summarized in Table 1.4.

We note that cellular dimensions are usually reported in micrometers ("microns"). Most biological channels have a conductance  $g$  on the order of 1 to 150 pS.

## 1.2 The fast Morris-Lecar model for the barnacle muscle fiber.

### 1.2.1 Description of the model.

Like most neural and muscle cells, the giant muscle fibers of the barnacle have a negative rest potential. Applying a positive current therefore has a depolarizing effect. Careful experiments have shown that current injections of various strengths can lead to complicated electrical behaviour, in particular to oscillations that may either be sustained or die out after some time.

Further experiments have shown that the giant muscle fiber of the barnacle contains primarily voltage gated  $K^+$  and  $Ca^{2+}$  currents but there is also a separate  $K^+$  current that is activated by intracellular  $Ca^{2+}$ , a so-called  $K_{Ca}^+$  - current. The voltage - gated currents are always activating, i.e. their  $f_\infty(V)$  functions are monotonously increasing, starting from near 0 for low values of  $V$  and tending to 1 for large values of  $V$ .

Morris and Lecar [8] proposed a simple model to explain the observed electrical behaviour. It involves only a fast activating  $Ca^{2+}$  current, a somewhat slower  $K^+$  current and a passive leak. More precisely, it models into two equations:

$$C \frac{dV}{dt} = -g_{Ca} m_\infty (V - V_{Ca}) - g_K w (V - V_K) - g_L (V - V_L) + I_{app} \quad (1.13)$$

$$\frac{dw}{dt} = \frac{\phi(w_\infty - w)}{\tau} \quad (1.14)$$

The equations (1.13,1.14) are called the *fast Morris-Lecar equations*.

In these expressions  $V_{Ca}$  and  $V_K$  are the reversal potentials for  $Ca^{2+}$  and  $K^+$ , respectively;  $g_{Ca}$  and  $g_K$  are the maximum conductances for  $Ca^{2+}$  and  $K^+$ , respectively. The state variable  $w$  represents the fraction of open  $K^+$  channels. Morris and Lecar assumed that  $Ca^{2+}$  is fast activating, in the sense that its fraction  $m$  of open channels converges almost instantaneously to its  $V$  - dependent equilibrium value  $m_\infty$ . Therefore there is no differential equation for  $m$  and in (1.13)  $m$  is replaced by its equilibrium value  $m_\infty$ . Next,  $V_L$  is the reversal potential for a leak current (a lumped approximation for all ions that contribute to a lesser degree to the dynamics of the neuron) for which the conductance  $g_L$  is small but fixed.

The functions

$$m_\infty = 0.5 \left( 1 + \tanh \frac{V - v_1}{v_2} \right) \quad (1.15)$$

$$w_\infty = 0.5 \left( 1 + \tanh \frac{V - v_3}{v_4} \right) \quad (1.16)$$

represent the equilibrium open fractions for the  $Ca^{2+}$  and  $K^+$  currents, respectively. The activation time for the  $K^+$  current is  $\frac{\tau}{\phi}$  where

$$\tau = \frac{1}{\cosh \frac{V - v_3}{2v_4}} \quad (1.17)$$

A representative set of parameters is given in Table 1.5.

In Figure 1.1 we present  $m_\infty$  as a function of  $V$ , where  $V$  is measured in mV. A function with this shape is called a *sigmoid* function. We note that  $m_\infty(V)$  is monotonously increasing,  $v_1$  is the (unique) potential for which  $m_\infty = 0.5$  and  $m_\infty(V)$  is close to 0 (respectively, 1) for small (respectively, large) values of  $V$ .

Parameter	Value
$C$	$20\mu F/cm^2$
$V_K$	$-84$ mV
$g_K$	$8$ mS / $cm^2$
$V_{Ca}$	$120$ mV
$g_{Ca}$	$4.4$ mS / $cm^2$
$V_L$	$-60$ mV
$g_L$	$2$ mS / $cm^2$
$v_1$	$-1.2$ mV
$v_2$	$18$ mV
$v_3$	$2$ mV
$v_4$	$30$ mV
$\phi$	$0.04/ms$

Table 1.5: Parameter values for the fast Morris-Lecar model.

We note that

$$\frac{dm_\infty(V)}{dV} = \frac{0.5}{\cosh^2\left(\frac{V-v_1}{v_2}\right)} \frac{1}{v_2},$$

and hence

$$\frac{dm_\infty(V)}{dV}(v_1) = \frac{1}{2v_2},$$

Hence the value of  $v_2$  determines the steepness of the sigmoid curve. For small (respectively, large) values of  $v_2$  (always positive!) the sigmoid function increases sharply (respectively slowly) near  $v = v_1$ . In fact, sigmoid functions like this with small  $v_2$  are often used to approximate the Heaviside function which is equal to zero if  $V < v_1$  and equal to 1 if  $V \geq v_1$ .

Now consider the contribution of the term  $-g_{Ca}m_\infty(V - V_{Ca})$  in (1.13). We represent it in Figure 1.2. We see that for large values of  $V$  the dependence on  $V$  is nearly linear. This is understandable since for large values of  $V$ ,  $m_\infty(V)$  is close to 1 and hence constant. For this reason, the  $Ca^{2+}$  current is called a rectifier in the jargon of circuit theory.

The behaviour of  $w_\infty(V)$  as a function of  $V$  is very similar to that of  $m_\infty$  (another sigmoid function). Nevertheless, the contribution of the  $K^+$  term in (1.13) is more complicated because of the time dependence of  $w$ . This function reaches its equilibrium value only after some delay; for this reason the  $K^+$  current is called a delayed rectifier.

### 1.3 Exercises

1. Compute the Nernst potential for  $K^+$ ,  $Na^+$ ,  $Cl^-$  in the squid giant axon and in a mammalian neuron (use Table 1.3.)
2. A bottle of Gerolsteiner mineral water contains 0.75 liters and the concentration in gram/liters is 118 for sodium, 11 for potassium, 348 for calcium, and 40 for chlorine. How many mol of each substance does the bottle contain?
3. A hamburger contains 375 large calories and 1 large calorie is equivalent to 4810 J. My weight is 75 kg and  $g = 9.81 \frac{m}{s^2}$ . How high can I climb after eating an hamburger?
4. My car consumes 8 liters of fuel per 100 kilometers. The relative density of the fuel is 0.75. It consists of carboretted hydrogens composed of  $C$  and  $H$  molecules. We assume

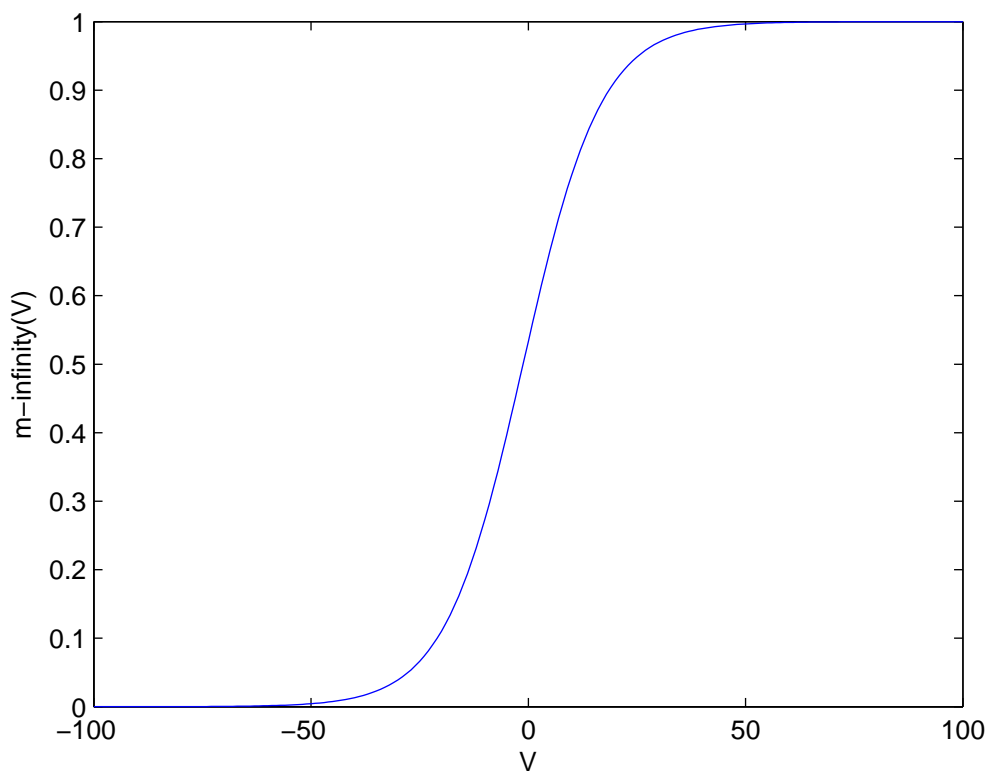


Figure 1.1: Fast Morris-Lecar:  $m_{\infty}$  as a function of  $V$ .

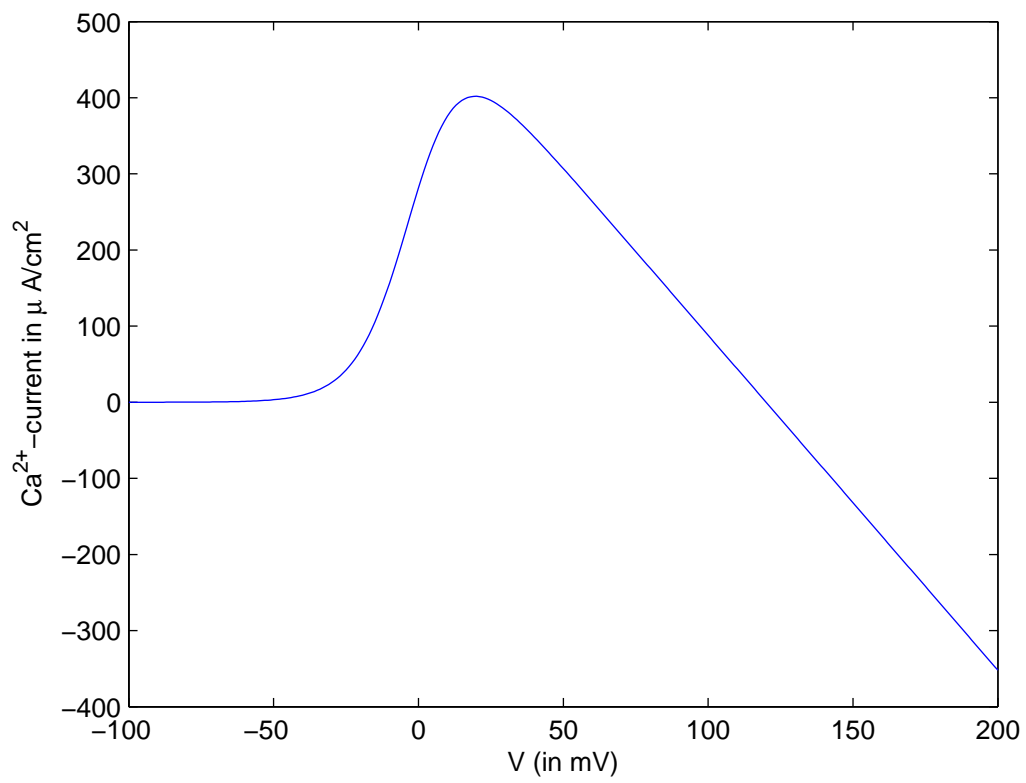


Figure 1.2: Fast Morris-Lecar: Contribution of the  $\text{Ca}^{2+}$  current as a function of  $V$ .

that the ratio is approximately 2  $H$  molecules for every  $C$  molecule (since fuel is a mixture of carboretted hydrogens, this can only be an approximation). Compute my  $CO_2$  emission when I drive 100 kilometers.

5. The rotor blades of a wind turbine have a length of 10m and the wind blows at a speed of 50 km/h. The relative density of air is 1.293 g/l. Suppose that the wind turbine has an efficiency of 40 %, i.e. it captures 40 % of the kinetic energy of the air that in unperturbed circumstances would blow through the disk formed by the rotating blades. Now:
  - (a) Compute the energy production of the turbine in kilowatts.
  - (b) The energy production is proportional to which power of the wind velocity?
6. Write a Matlab program that reproduces Figure 1.1.
7. Write a Matlab program that reproduces Figure 1.2.
8. Consider the ML model in (1.13) and (1.14) and call this model I. Now introduce model II which is the expanded form of model I and is explicitly given by

$$\begin{cases} C \frac{dV}{dt} &= -g_{Ca}m(V - V_{Ca}) - g_K w(V - V_K) - g_L(V - V_L) + I_{app} \\ \frac{dw}{dt} &= \frac{\phi(w_\infty - w)}{\tau} \\ \frac{dm}{dt} &= \frac{m_\infty - m}{\tau_1} \end{cases} \quad (1.18)$$

Here  $\tau_1$  is a new constant whose value determines how fast  $m$  converges to its ( $V$  - dependent) steady state value  $m_\infty$ .

- (a) Prove (analytically) that models I and II have the same equilibria (it being understood that in model II  $m = m_\infty$  in an equilibrium point).
- (b) Prove (analytically) that models I and II have the same limit points.
- (c) Show by numerical computations that models I and II do not have the same Hopf points (take  $\tau_1 = 0.01$ .)

## Chapter 2

# Computational study of the Morris-Lecar equations

In this chapter we study the dynamical properties of the Morris-Lecar model, from elementary simulations up to codimension 2 bifurcations and their interactions with codimension 1 bifurcations.

### 2.1 Simulation study of the fast Morris-Lecar equations.

It is not possible to solve the system (1.13,1.14) analytically. However, we can make a numerical study. We start with the time evolution of the system for several values of  $I_{app}$ . Current in the fast Morris-Lecar model is expressed in  $\mu\text{A}/\text{cm}^2$ . For simplicity, we assume that the cell has a total surface of  $10^{-6}\text{cm}^2$ , so that  $1 \mu\text{A}/\text{cm}^2$  corresponds to 1 pA of total current. So we will measure the currents in (1.13) in pA. Voltage is measured in mV and time in ms. Hence the capacitance must be measured in  $(\text{pA} \times \text{ms})/\text{mV} = \text{pF}$ . From Table 1.5 we deduce that the whole-cell capacitance is  $10^{-6} \times 20\mu\text{F} = 20 \text{ pF}$ . Next, the conductances must be measured in  $\text{pA}/\text{mV} = \text{nS}$ . From Table 1.5 we deduce that the whole cell conductance for  $\text{K}^+$  is  $8 \cdot 10^{-6}\text{mS} = 8\text{nS}$ . The other quantities in Table 1.5 can be treated similarly or present no difficulties, so that we finally obtain Table 2.1:

Parameter	Value
C	20
$V_K$	-84
$g_K$	8
$V_{Ca}$	120
$g_{Ca}$	4.4
$V_L$	-60
$g_L$	2
$v_1$	-1.2
$v_2$	18
$v_3$	2
$v_4$	30
$\phi$	0.04

Table 2.1: Parameter values for the whole-cell fast Morris-Lecar model in compatible units.

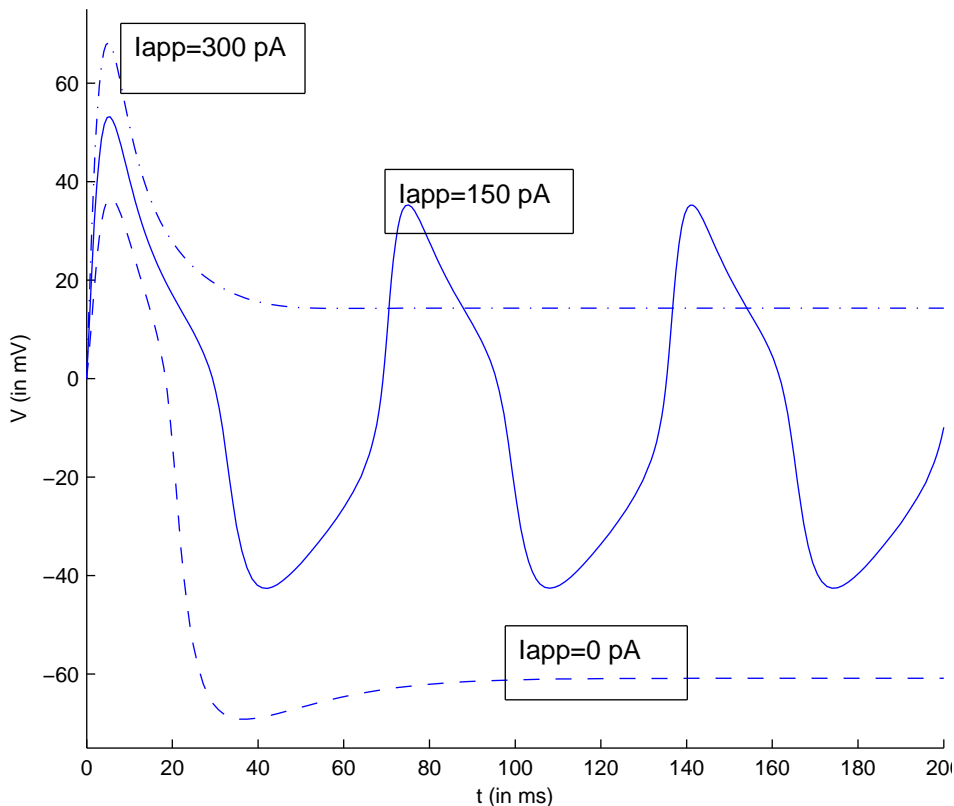


Figure 2.1: Simulation of the fast Morris-Lecar system with  $I_{app} = 0$  pA (dashed line),  $I_{app} = 150$  pA (solid line) and  $I_{app} = 300$  pA (dash-dotted line).

In Figure 2.1 we present three numerical solutions of (1.13,1.14) with starting values  $V = 0, w = 0$ . For  $I_{app} = 0$  we find the dashed curve. It is clear that the system converges to a stable equilibrium where  $V$  is close to  $-60$ . Similar experiments with other starting values for  $V, w$  always lead to the same equilibrium, the potential of which is called the rest potential of the system. For  $I_{app} = 300$  we find the dash-dotted curve which also converges to a stable equilibrium where  $V$  is close to  $+20$  mV. For  $I_{app} = 150$  we find the solid curve which does not converge to an equilibrium but oscillates periodically after a transient.

In Figure 2.2 we present a phase portrait in the case  $I_{app} = 0$ . This means that we plot several orbits, corresponding to different starting values in the phase space, i.e. in the space of state variables, where time is not visible. Phase portraits are very useful in systems with two state variables such as the fast Morris-Lecar system (planar systems) or even in three-dimensional systems but their use is limited in higher dimensions.

It is clear that all four trajectories converge to the same equilibrium where (approximately)  $V = -60.999659, w = 0.015325705$ .

It is instructive to draw similar phase portraits for  $I_{app} = 150$ ; one then sees that all trajectories converge to the same closed curve, which represents a periodic orbit.

Similarly, in phase portraits for  $I_{app} = 300$  all trajectories converge to the same equilibrium where (approximately)  $V = 14.301492, w = 0.6942484$ .

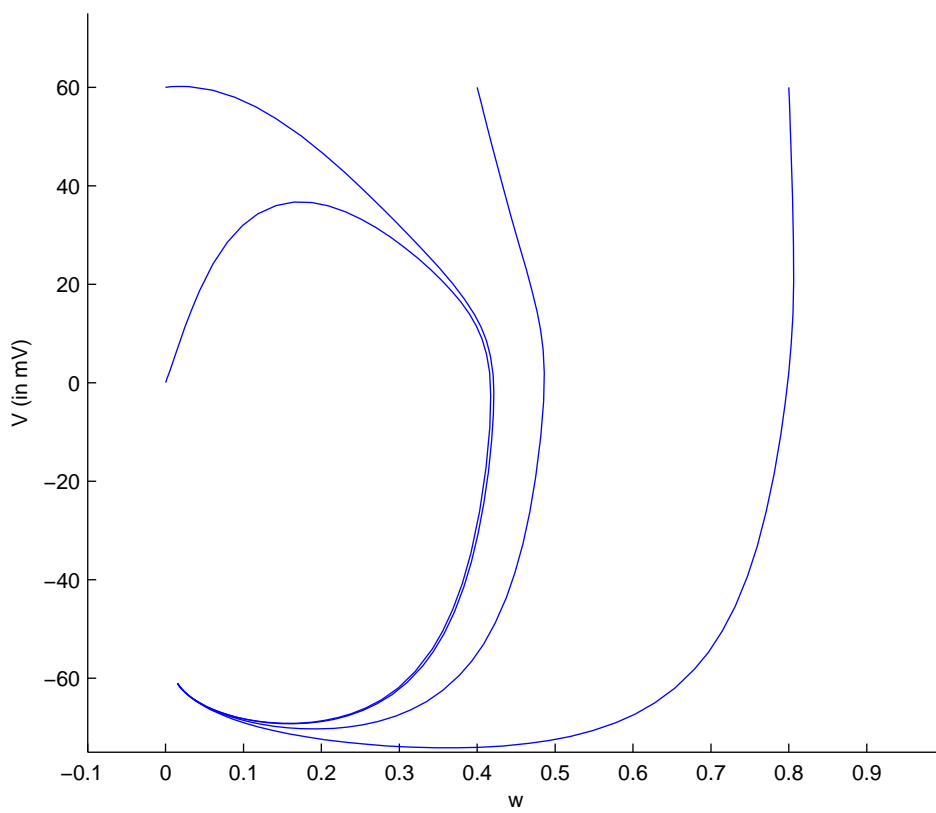


Figure 2.2: Phase plane simulation of the fast Morris-Lecar system with  $I_{app} = 0$  pA and four different starting values of  $V, w$

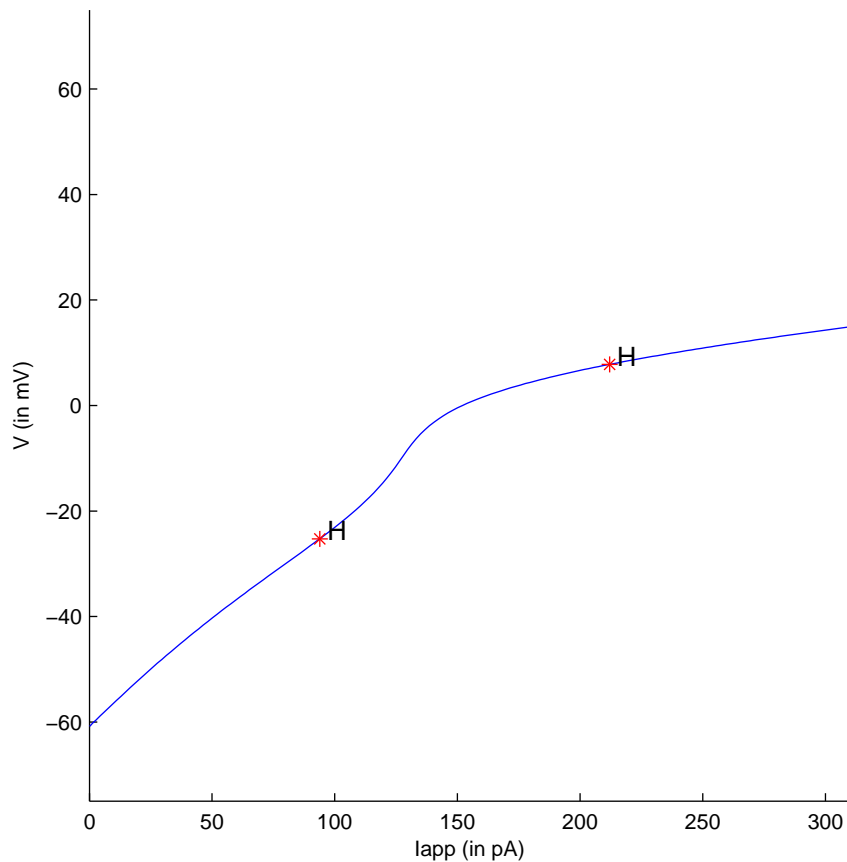


Figure 2.3: A branch of equilibria in the fast Morris-Lecar system.

### 2.1.1 Stable and unstable equilibria and their continuation

From §2.1 it is clear that in the fast Morris-Lecar model for a cell with a surface of  $10^{-6}\text{cm}^2$ ,  $0 \text{ pA} \leq I_{app} \leq 300 \text{ pA}$  and all other parameters as in Table 1.5, there is always a unique equilibrium in the relevant state vector range. However, it is stable for both small and large values of  $I_{app}$  but unstable for many intermediate values. For these intermediate values, stable limit cycles seem to exist. Hence we may expect that we can numerically continue the equilibrium states of the system under variation of the parameter  $I_{app}$  and, hopefully, detect bifurcation points where the stability changes and periodic orbits can be born.

For practical purposes, we start with time integration to compute a stable equilibrium for  $I_{app} = 0$ . We start with any starting values, e.g.  $V = w = 0$  and integrate for some time, e.g. 1000 units of time (ms). At the end we find  $V = -60.85456779$ ,  $w = 0.0149139691$ . From this point we start the numerical continuation of equilibria, choosing  $I_{app}$  as the free parameter and letting it vary from 0 to 300. As a result we obtain the simple picture in Figure 2.3.

As expected, the eigenvalues of the Jacobian matrix initially have negative real parts. In fact, they form a conjugate pair of complex eigenvalues. This pair crosses the imaginary axis at the first Hopf (H) point in Figure 2.3 where  $V = -25.270105$ ,  $w = 0.139673$ ,  $I_{app} = 93.857618$ . Interestingly, the first Lyapunov coefficient is  $5.220222e - 004 > 0$ . This implies that the

Hopf bifurcation is subcritical, i.e. the periodic orbits are born unstable. The unstable equilibria are continued further and regain stability at the second Hopf point in Figure 2.3 where  $V = 7.800664$ ,  $w = 0.595491$ ,  $I_{app} = 212.018816$ . The first Lyapunov coefficient is  $5.451010e - 004$ , so that this Hopf point is again subcritical and so unstable periodic orbits are born.

### 2.1.2 Continuation of periodic orbits

At first sight, it is rather unexpected to find unstable periodic orbits in the fast Morris-Lecar model, since in §2.1 we found stable periodic orbits for  $I_{app} = 150$ . However, this is not a contradiction since both stable and unstable periodic orbits may exist. In addition, we note that unstable periodic orbits cannot be found easily by direct time integration.

To compute the unstable periodic orbits, we start their continuation from the Hopf points detected in §2.1.1. The periodic orbits born at the first Hopf point ( $I_{app} = 93.857618$ ) exist for decreasing values of  $I_{app}$ . For  $I_{app} = 88.2948$  (approximately) they reach a fold bifurcation of limit cycles (LPC), become stable and continue for increasing values of  $I_{app}$ . Similarly, the periodic orbits born at the second Hopf point ( $I_{app} = 212.018816$ ) exist for increasing values of  $I_{app}$ . For  $I_{app} = 216.8998$  (approximately) they reach a fold bifurcation of limit cycles (LPC), become stable and continue for decreasing values of  $I_{app}$ . The equilibria and unstable periodic orbits together are presented in Figure 2.4.

The stable periodic orbits that are born at the LPC (fold bifurcation of limit cycles) at  $I_{app} = 88.2948$  can be continued numerically and then connect to those born at the other LPC at  $I_{app} = 216.8998$ . The equilibria and stable periodic orbits together are presented in Figure 2.5.

We note that there are two ranges for  $I_{app}$ , namely  $[88.2948, 93.857618]$  and  $[212.018816, 216.8998]$  where a stable equilibrium, an unstable periodic orbit, and a stable periodic orbit coexist. This phenomenon would be hard to detect by direct simulation. To illustrate this, consider Figure 2.6 which was drawn for  $I_{app} = 91$ . One sees that "most" orbits converge to the stable periodic orbit. However, there is a small region, which includes the point  $(-18, 0.19)$  from where the orbits converge to a stable equilibrium. So this stable equilibrium has only a small domain of attraction.

The boundary between the two domains of attraction is the unstable periodic orbit, drawn as a thick dashed line in Figure 2.6.

## 2.2 Two-parameter study of the fast Morris-Lecar model.

### 2.2.1 Bogdanov-Takens points.

We recall that in §2.1.1 two subcritical Hopf points were detected on a branch of equilibria in which  $I_{app}$  (the externally applied current) was the free parameter. We can expect, of course, that this behaviour depends on the other parameters of the system. In general, it is usually not feasible to study the complete bifurcation picture as a function of all parameters of the system. However, we can at least free a second parameter and make a two - parameter study.

We note that in practice parameters are often not known with great precision. Since the bifurcations depend on the parameter values, a bifurcation study and its comparison with experiments can help to compute the parameters of the system.

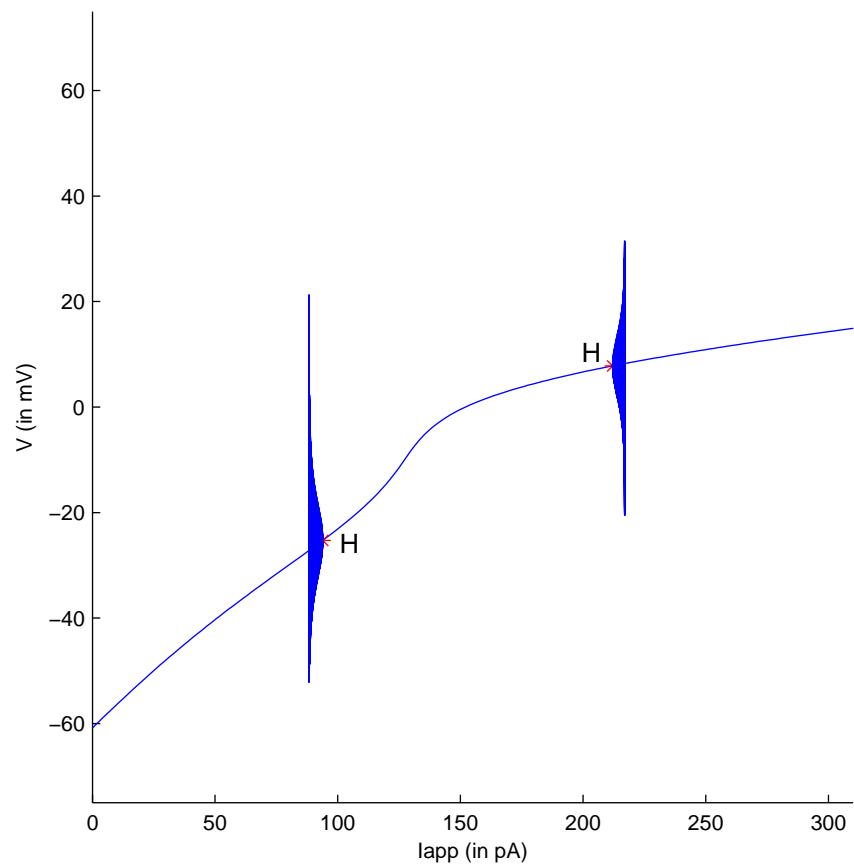


Figure 2.4: Equilibria and unstable periodic orbits in the fast Morris-Lecar system.

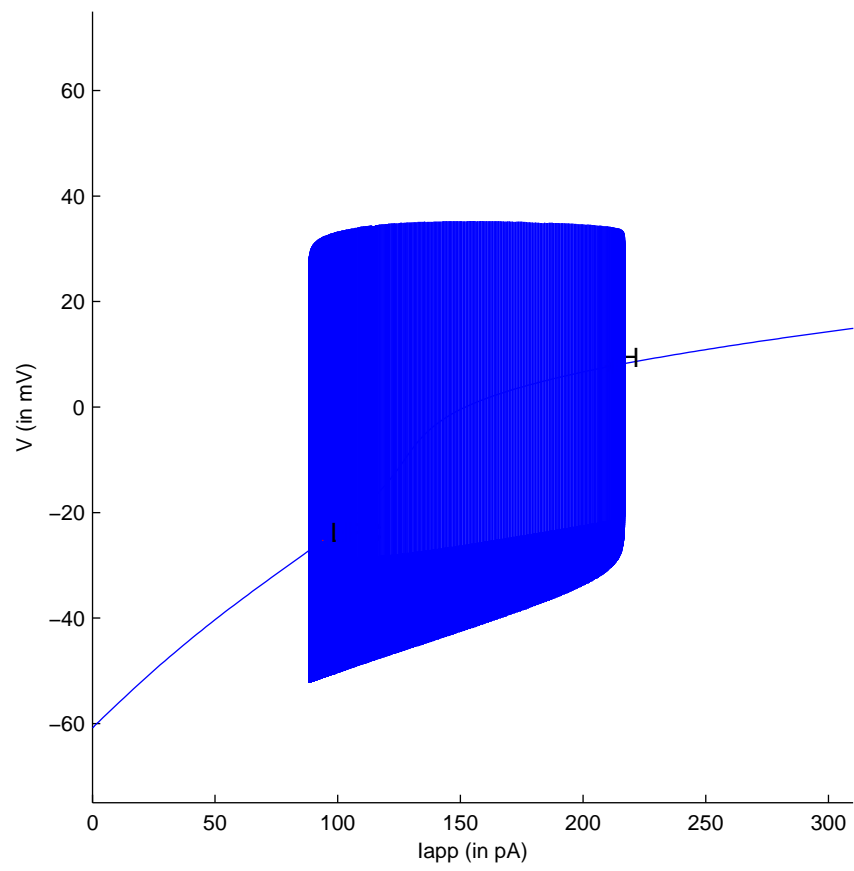


Figure 2.5: Equilibria and stable periodic orbits in the fast Morris-Lecar system.

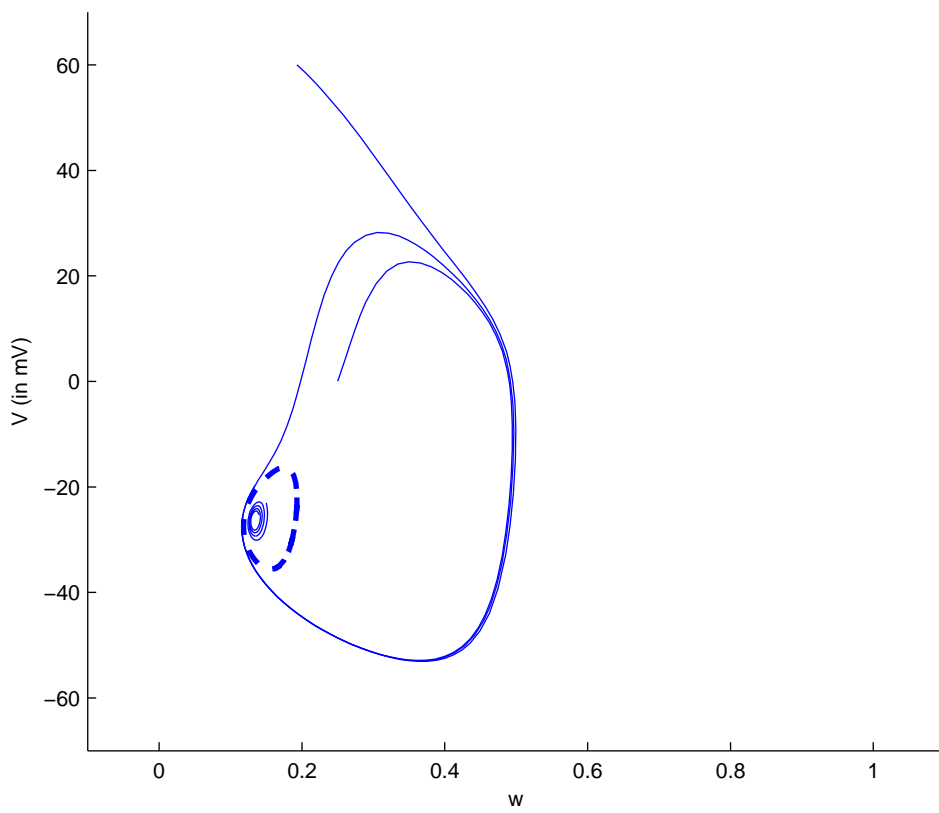


Figure 2.6: Converging orbits in the fast Morris-Lecar system for  $I_{app} = 91$ .

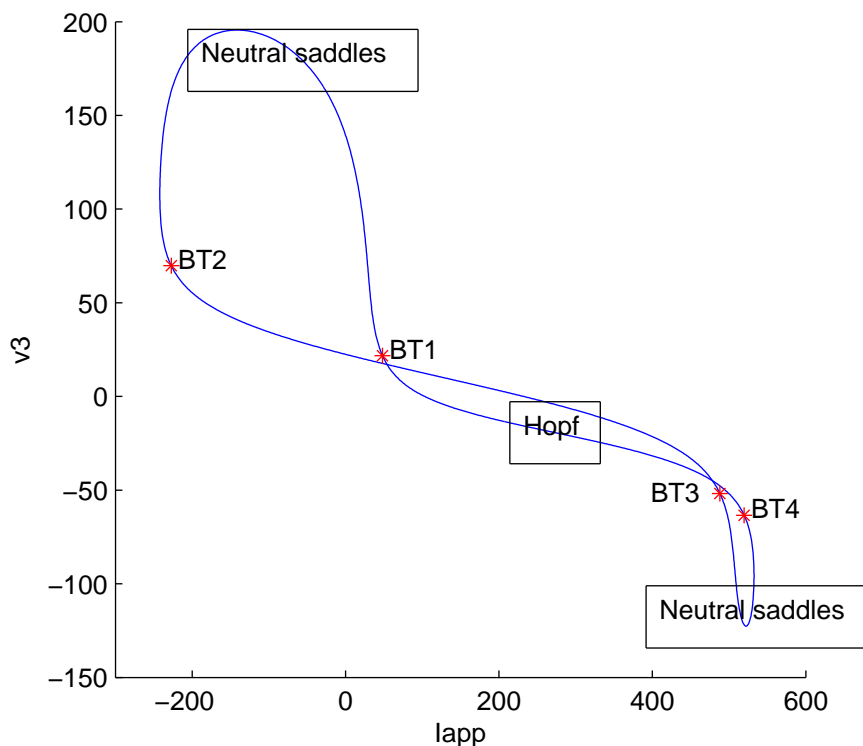


Figure 2.7: A curve of Hopf points in the fast Morris-Lecar model.

As an example, we make a simple study of the fast Morris-Lecar equations with two free parameters  $I_{app}$ ,  $v_3$  (we might imagine that in an experiment the value of  $v_3$  is not known accurately and that we want to obtain information by studying how the value of  $v_3$  influences the bifurcation behaviour).

Starting from any of the Hopf points detected in §2.1.1 we can compute a family of Hopf points with free parameters  $I_{app}$ ,  $v_3$ . It turns out, interestingly that we obtain a closed curve in the  $(I_{app}, v_3)$  - space which contains 4 Bogdanov-Takens (BT) points, see Figure 2.7.

BT points are equilibria in which the Jacobian matrix has two zero eigenvalues. They are found generically on curves of Hopf points (when the two pure imaginary eigenvalues  $\pm i\omega$  collide) and on curves of limit points (when a second eigenvalue becomes zero). Moreover, in two-parameter problems BT points are origins for branches of orbits homoclinic to hyperbolic saddle (HHS).

Mathematically it is convenient to determine a Hopf curve as a curve of equilibria for which there is a pair of eigenvalues with sum zero. This, however, includes not only Hopf points but also points with two real eigenvalues  $\pm r$  with opposite sign. Such points are called neutral saddles. On the closed curve in Figure 2.7 the BT points separate the Hopf points from the neutral saddles. Hopf points are found on the curve pieces BT1-BT3 and BT4-BT2. Neutral saddle points are found on the curve pieces BT1-BT2 and BT3-BT4. We note that the first Lyapunov coefficient is positive in all Hopf points, so all Hopf bifurcations are subcritical.

It is clear that the information contained in Figure 2.7 can help to find the parameters

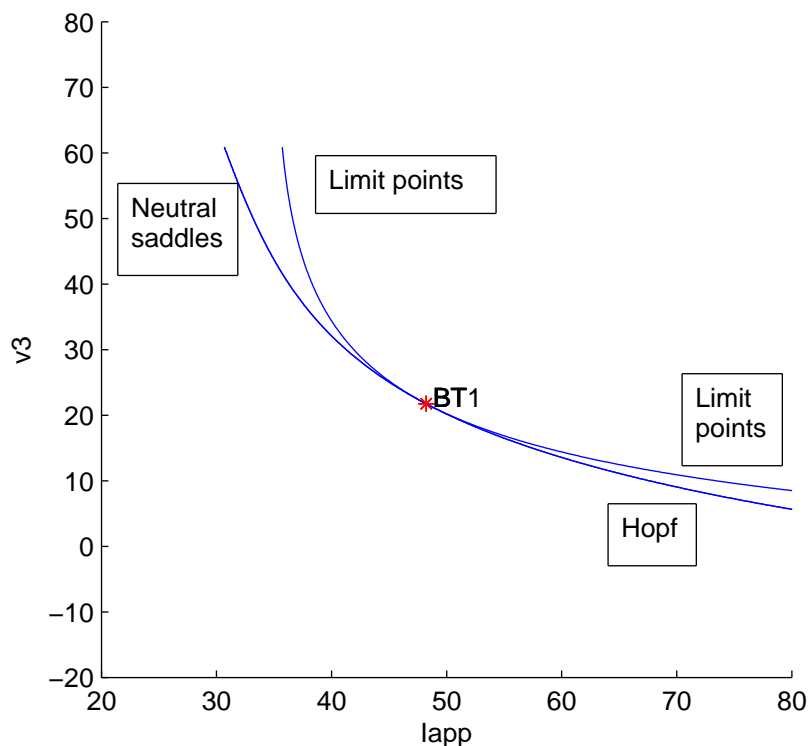


Figure 2.8: Hopf points and Limit points meeting in a BT point.

of the system. For example, if we knew all parameters except  $v_3$  but knew that its value is between the values for which we find BT4 and BT2 (a very reasonable assumption) then an experiment with variable  $I_{app}$  can provide the Hopf points and so determine the value of  $v_3$ .

In Figure 2.8 we present a close-up of the Hopf-Neutral Saddle curve and the limit point curve that meet (tangentially) in BT1.

### 2.2.2 Generalized Hopf points.

A slightly different set of parameters has also been considered extensively in the literature. We give it in Table 2.2;  $I_{app}$  and  $v_3$  are varied in the tests.

A Hopf curve for this case similar to that in Figure 2.7 is presented in Figure 2.9.

The only qualitative novelty is the presence of the Generalized Hopf points GH1 and GH2. In these points the first Lyapunov value vanishes. The Hopf points are supercritical (negative first Lyapunov coefficient) in the (relatively) small part of the curve between GH1 ( $v_3 = 2.0215262$ ,  $I_{app} = 255.90695$ ), and GH2 ( $v_3 = -24.596518$ ,  $I_{app} = 474.37505$ ); they are subcritical (positive first Lyapunov coefficient) in all other Hopf points.

Another important aspect of GH points in two-parameter problems is that in them curves of limit point bifurcations of limit cycles (LPC) are born. In Figure 2.10 we show the curve of LPC points that ends in GH1. We note that it is tangential to the Hopf curve.

Parameter	Value
$C$	5
$V_K$	-80
$g_K$	8
$V_{Ca}$	120
$g_{Ca}$	4
$V_L$	-60
$g_L$	2
$v_1$	-1.2
$v_2$	18
$v_4$	17.4
$\phi$	$\frac{1}{15}$

Table 2.2: Parameter values for the whole-cell fast Morris-Lecar model in compatible units.

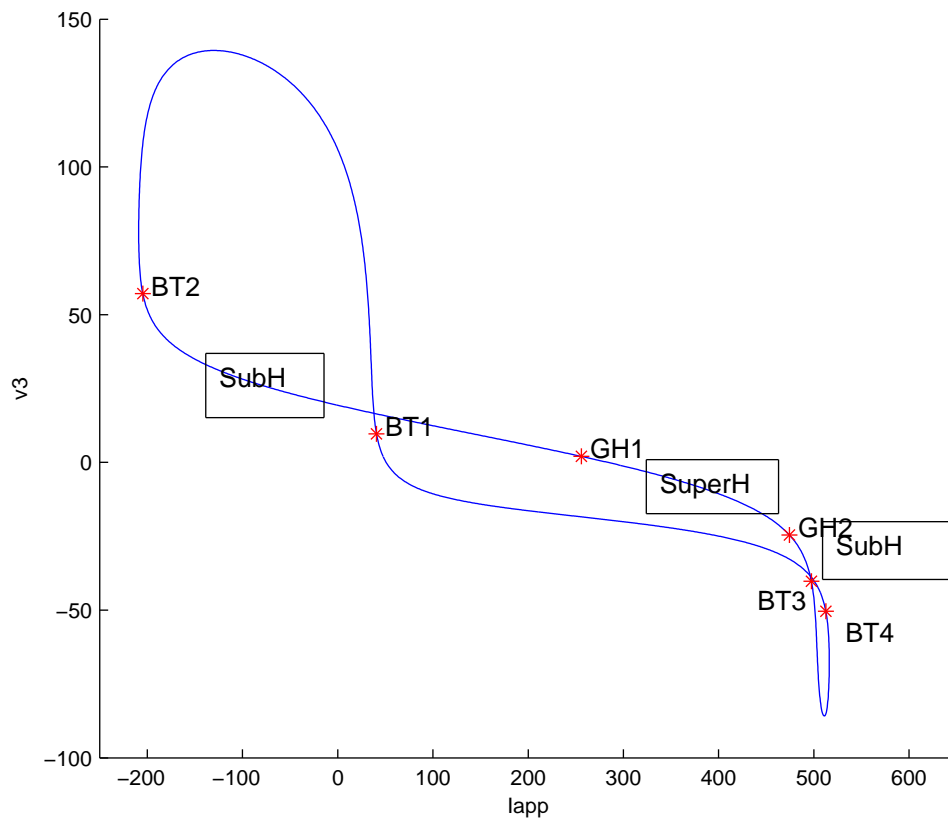


Figure 2.9: A curve of Hopf points in the fast Morris-Lecar model.

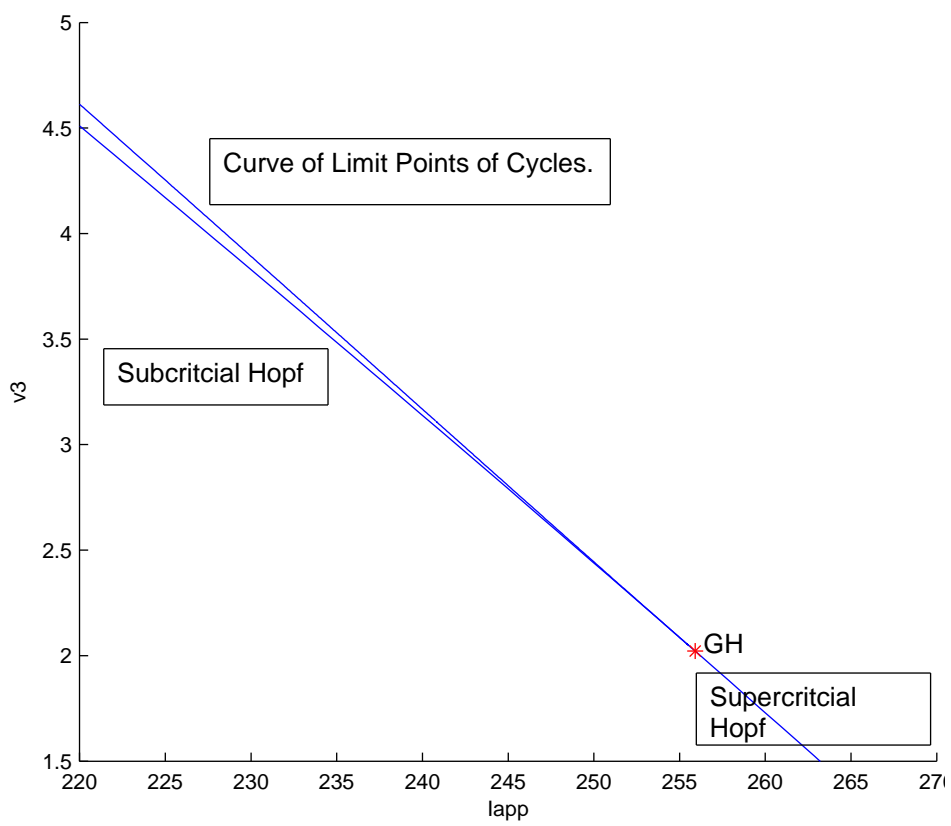


Figure 2.10: A curve of limit points of cycles that ends in a GH point.

## 2.3 Excitability in the fast Morris-Lecar model.

Hodgkin and Huxley [4] found in their experiments on the giant axon of the squid that when the input current was increased until the equilibrium state lost its stability, then the loss of stability could happen in two different ways. In the first case, which they called Type I excitability, the equilibrium was replaced by a periodic oscillation that could have an arbitrarily low frequency, i.e. an arbitrarily long period (the frequency being the inverse of the period). In the second case, which they called Type II excitability, the equilibrium was always replaced by a periodic oscillation with a frequency in a bounded range (i.e. a period in a bounded range).

### 2.3.1 Type I excitability.

In the fast Morris-Lecar model we can find and study Type I excitability in a relevant parameter range. The parameters different from  $v_3$  and  $I_{app}$  are given in Table 2.2. The Bogdanov-Takens point BT1 in Figure 2.9 is found for  $v_3 = 9.673493$ . For slightly larger values of  $v_3$  the stability of the equilibria is lost for increasing values of  $I_{app}$  by a limit point bifurcation. In particular, for  $v_3 = 15$  the limit point is found for  $I_{app} = I_{app,0} \simeq 38.762757$ . By time integration of (1.13,1.14) for values of  $I_{app}$  larger than  $I_{app,0}$  (take  $I_{app} = 45$ ) we find stable periodic orbits whose period tends to infinity when  $I_{app}$  tends to  $I_{app,0}$ . In fact, by a continuation of periodic orbits we can plot the period  $T$  of the orbit as a function of  $I_{app}$  and obtain Figure 2.11.

In Figures 2.12, 2.13 and 2.14 we present the time evolution of  $V$ , respectively  $w$  and both  $V, w$  for  $v_3 = 15$ ,  $I_{app} = 38.7664$  in time rescaled to  $[0, 1]$  (the period is 566.1981, so the real time scale is from 0 to 566.1981 ms). We note that most of the time the orbit is close to the pair  $V = -30.3775$ ,  $w = 0.0054$  near the equilibrium value at the limit point; this quiescent state is interrupted by a spike. The long period is explained by the fact that the system stays near the equilibrium value for a long time, briefly spikes and then returns to the neighborhood of the equilibrium value. In Figure 2.15 we show the orbit in phase space; the most remarkable thing to observe in this Figure is that the phase space orbit does not clearly indicate that we deal with a spiking orbit. It can be demonstrated, however, by doing time integration with small time intervals and extending the integration many times.

It can be shown that for  $I_{app} = I_{app,0}$  (the limit point) the system has a homoclinic-to-saddle-node orbit, i.e. an orbit along which the system tends to the same saddle-node equilibrium if time tends to  $\pm\infty$ .

### 2.3.2 Type II excitability.

In the fast Morris-Lecar model we can find and study Type II excitability in a relevant parameter range. In fact, we found it already in §2.1.1 and §2.1.2. The parameters different from  $I_{app}$  are given in Table 2.1. We recall from §2.1.1 that stable equilibria exist for  $I_{app} < 93.857618$ . They lose stability for that value of  $I_{app}$  (a subcritical Hopf point) and are replaced by stable periodic orbits which exist for  $88.2948 < I_{app} < 216.8998$  (as we saw in §2.1.2).

For  $I_{app} < 95$  the periods of the stable orbits are always between 89 and 137, so the loss of stability at the Hopf point always results into periodic orbits with a period, and hence a frequency, in a bounded range.

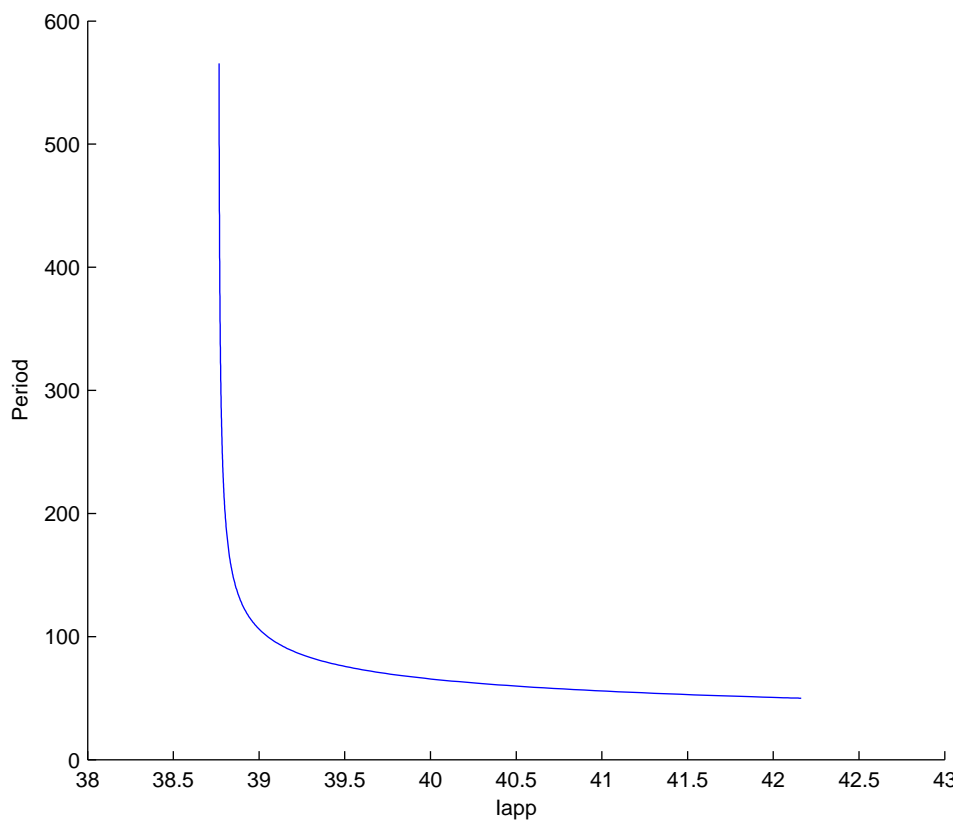


Figure 2.11: Type I spiking: Period as a function of  $I_{app}$  for constant  $v_3 = 15$ . The LP bifurcation on the equilibrium branch is found for  $I_{app} = 38.762752$ .

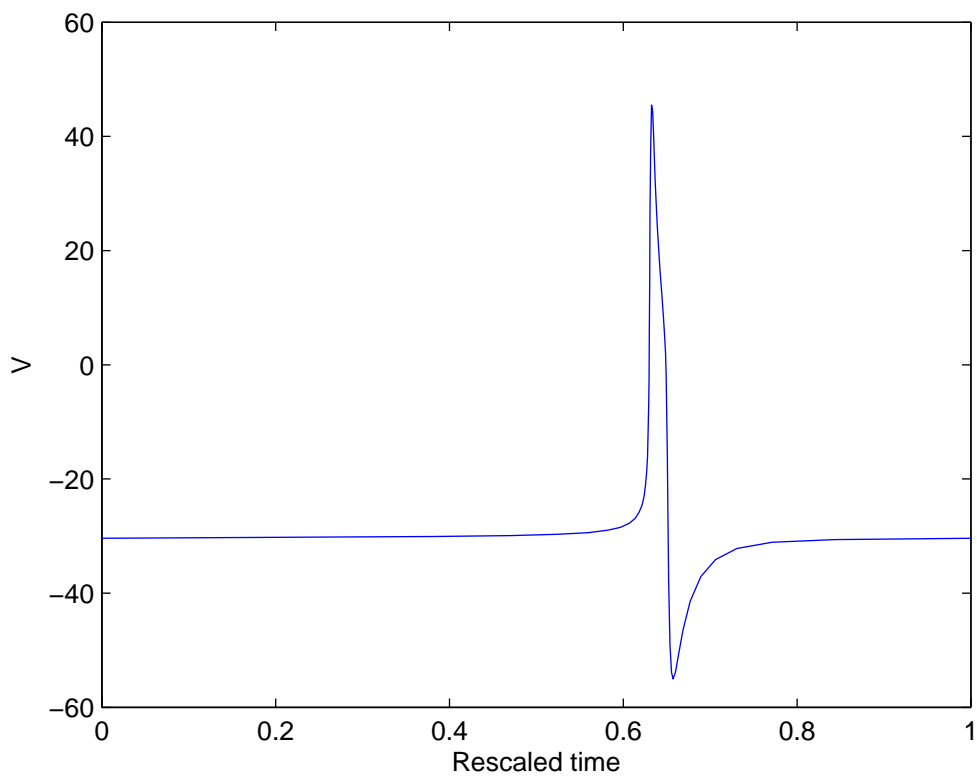


Figure 2.12: A spiking orbit for  $v_3 = 15$ ,  $I_{app} = 38.7664$ . Time is rescaled to  $[0, 1]$ .

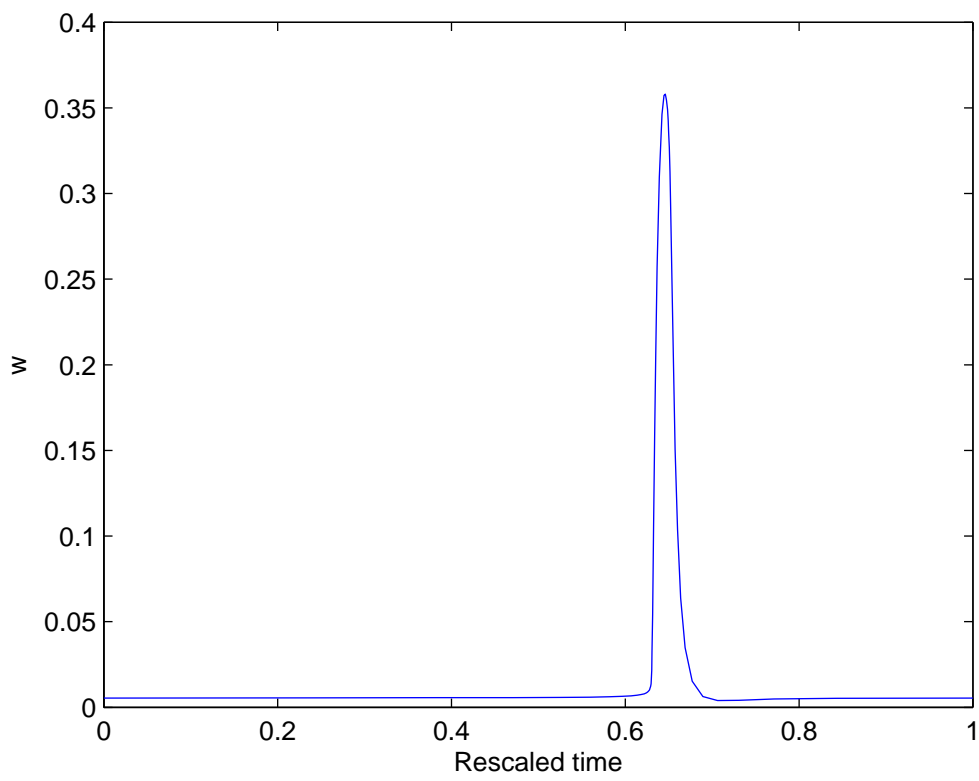


Figure 2.13: A spiking orbit for  $v_3 = 15$ ,  $I_{app} = 38.7664$ . Time is rescaled to  $[0, 1]$ .

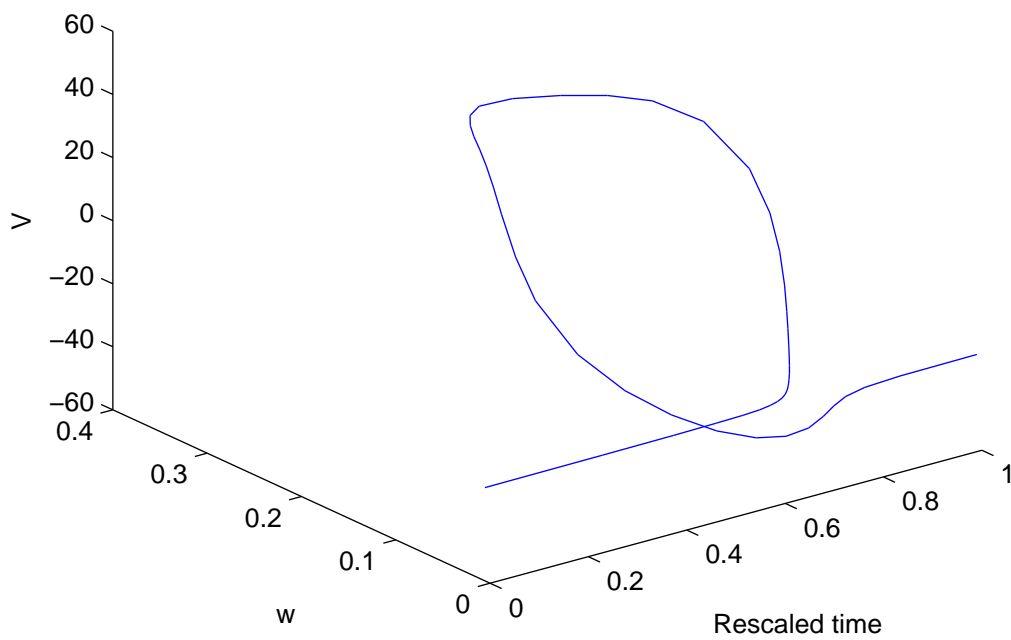


Figure 2.14: A spiking orbit for  $v_3 = 15$ ,  $I_{app} = 38.7664$ . Time is rescaled to  $[0, 1]$ .

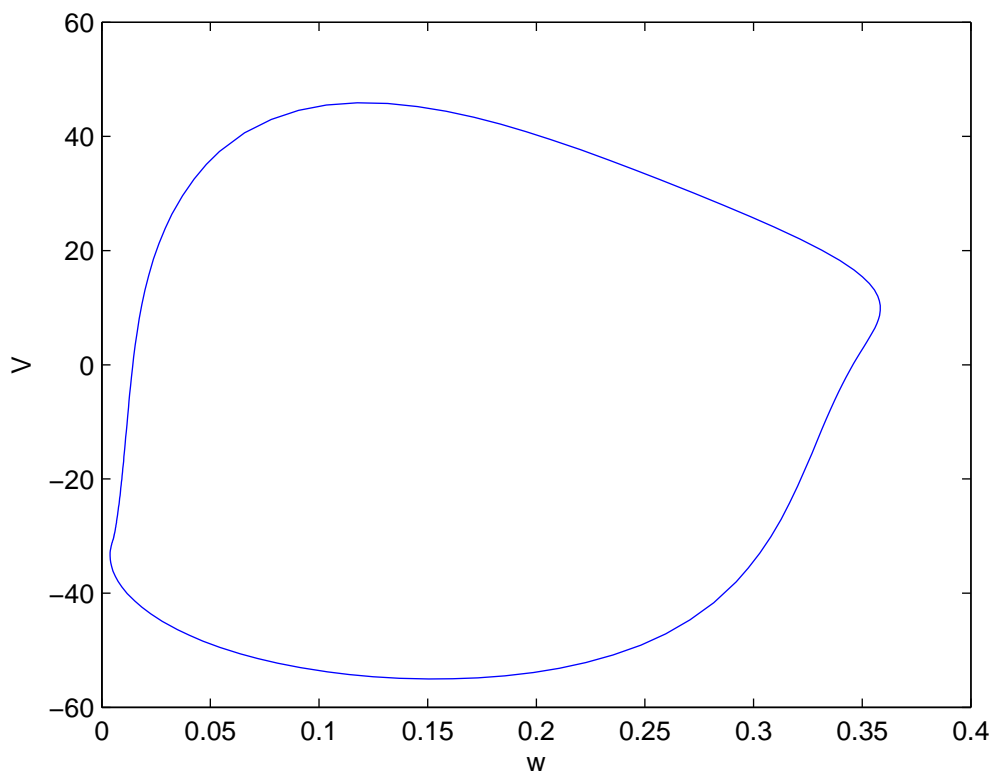


Figure 2.15: A spiking orbit in phase space for  $v_3 = 15$ ,  $I_{app} = 38.7664$ .

## 2.4 The slow-fast Morris-Lecar model for the barnacle muscle fiber.

### 2.4.1 Description of the slow-fast model.

As we noted in §1.2.1 the giant muscle fiber of the barnacle contains not only voltage gated  $K^+$  and  $Ca^{2+}$  currents (these were modeled by (1.13,1.14)), but there is also a separate but slower  $K^+$  current that is activated by intracellular  $Ca^{2+}$ , a so-called  $K_{Ca}^+$  - current. Morris and Lecar [8] observed that the barnacle muscle fiber could produce behaviour that was far more complicated than the periodic orbits and equilibria described in §1.2. They also observed that the behaviour by low levels of internal  $Ca^{2+}$  was different from that by high levels.

Morris and Lecar therefore produced several models to include the (slow) time evolution of the internal  $Ca^{2+}$  concentration. For simplicity, we consider here a variant introduced by Terman [10, 11]. It consists of

$$C \frac{dV}{dt} = y - g_{Ca} m_{\infty}(V - V_{Ca}) - g_K w(V - V_K) - g_L(V - V_L) + I_{app} \quad (2.1)$$

$$\frac{dw}{dt} = \frac{\phi(w_{\infty} - w)}{\tau} \quad (2.2)$$

$$\frac{dy}{dt} = \epsilon(k - V) \quad (2.3)$$

We note that to the system (1.13,1.14) we have now added a third variable  $y$  with the dimension of a current (picoAmperes) that is proportional to the internal  $Ca^{2+}$  concentration. Also, we have two new parameters,  $\epsilon$  and  $k$ . The latter is a sort of reversal potential:  $y$  is increasing if  $V < k$  and decreasing if  $V > k$ . Furthermore,  $\epsilon$  is a small number so that the rate of increase or decrease of  $y$  is always slow when compared to  $V$  and  $w$ . For this reason, the system (2.1,2.2,2.3) is called a slow-fast system. The subsystem (2.1,2.2) with frozen  $y$  is then called the fast subsystem. We note that it is, in fact, equivalent to (1.13,1.14) since we can incorporate  $y$  into  $I_{app}$  if  $y$  is fixed.

### 2.4.2 Bursting in the slow-fast model.

We now discuss the bursting phenomenon as it can often be observed in slow-fast systems and, indeed, was found by experimentalists in most excitable cells, e.g. [8]. In Figure 2.16 we show the time evolution of the slow-fast Morris-Lecar model. We start with the parameter values in Table 1.5, complemented by setting  $I_{app} = 0$ ,  $k = -25$ ,  $\epsilon = 0.001$ ; for simplicity we start with  $V = -60$ ,  $w = 0$ ,  $y = 0$ .

We see that after a transient, the model exhibits a periodic bursting. A burst consists of a large number of potential spikes which are fired off in rapid succession; between two bursts the system is quiet. A more detailed view of a burst is presented in Figure 2.17.

To understand this behaviour, it is useful to look at a 3D picture in phase space, see Figure 2.18. We note that in the slow-fast Morris-Lecar system  $y$  plays the same role as  $I_{app}$  in the fast system, but  $y$  is slowly varying instead of being constant. In Figure 2.18 we see that during one burst  $y$  oscillates between approximately 87 and 93. In §2.1.2 we saw that the fast system has a stable periodic orbit for  $I_{app} > 88.2948$  and a stable equilibrium for  $I_{app} < 93.857618$ . Between the two values we have bistability of the equilibrium and the

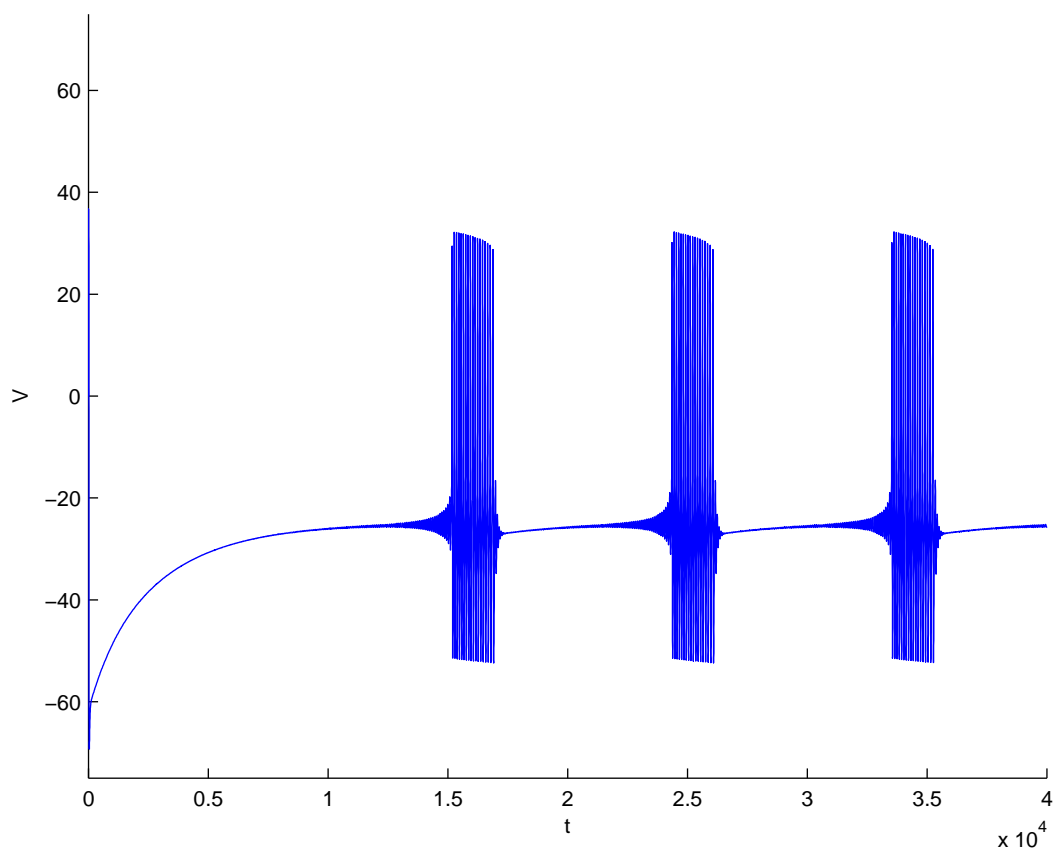


Figure 2.16: Time evolution of a bursting cell.

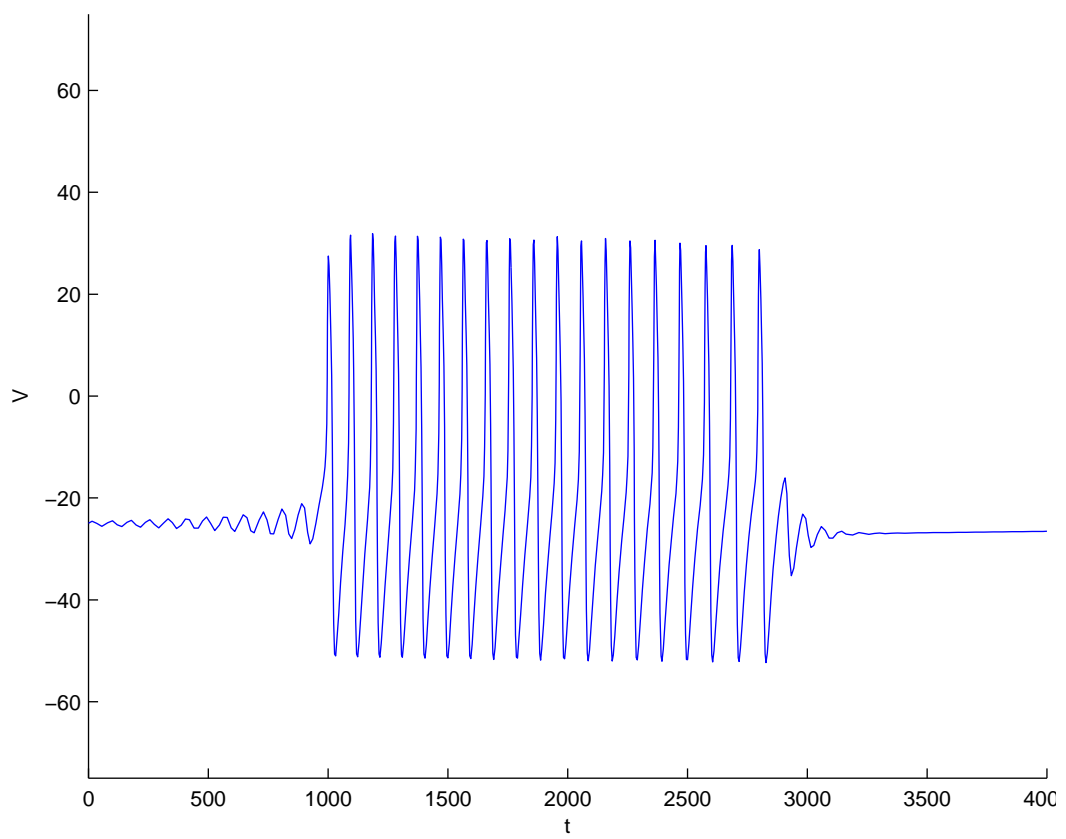


Figure 2.17: Detail of the time evolution of a bursting cell.

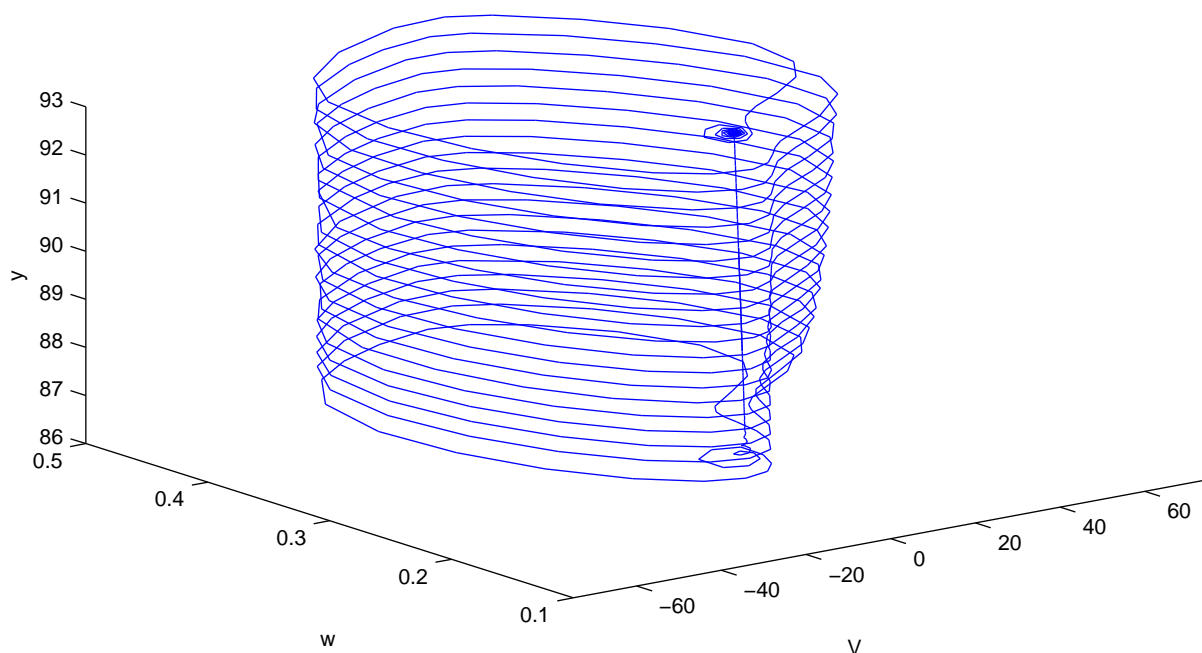


Figure 2.18: 3D view of the time evolution of a bursting cell.

periodic orbit. Now for small values of  $y$  the fast system rapidly converges to the stable equilibrium. However, in these equilibria we have  $V < k$ ; therefore, by (2.3) we have  $\frac{dy}{dt} > 0$ , i.e.  $y$  is (slowly) increasing. After some time,  $y$  approaches the value 93 and at some point the equilibrium loses stability. The fast system then jumps to the stable periodic orbit that is clearly visible in Figure 2.18. However, along this stable periodic orbit  $V$  predominantly takes values larger than  $k$  and this causes  $y$  to decrease. After some time,  $y$  approaches the value where the periodic orbit loses stability. The system then returns to the stable equilibrium and the whole cycle starts again.

We note that bursting can lead to the blue-sky catastrophe, when a parameter of the system is varied in such a way that the number of spikes in a burst tends to infinity in a bounded parameter range.

## 2.5 Exercises

1. Produce Figure 2.1, using MATCONT.
2. Produce Figures similar to 2.2 for  $I_{app} = 150$ , and for  $I_{app} = 300$ , using MATCONT. In the case of  $I_{app} = 150$ , demonstrate that orbits that start from within the limit cycle also converge to it.
3. The Morris-Lecar system (1.13,1.14) is planar, i.e. has two state dimensions. Therefore it can be useful to draw phase portraits. Draw the isoclines for the parameter values in Table 2.1 and  $I_{app} = 300$ . Do the same for  $I_{app} = 150$ . Can you draw conclusions on the existence of equilibria and periodic orbits?

4. Check the computations that provided Figures 2.3, 2.4 and 2.5.
5. Check the computations that produced Figure 2.6.
6. Consider a planar system

$$\begin{cases} \frac{dx}{dt} = f(x, y), \\ \frac{dy}{dt} = g(x, y) \end{cases}$$

Suppose that the isoclines  $f(x, y) = 0$ ,  $g(x, y) = 0$ , intersect transversally in the point  $(x_0, y_0)$  where all partial derivatives of  $f$  and  $g$  are nonzero. Suppose further that in  $(x_0, y_0)$  the isocline  $f = 0$  forms an angle  $\alpha$ , with  $0 < \alpha < \frac{\pi}{2}$  with the positive  $x$ - axis and the isocline  $g = 0$  forms an angle  $\beta$ , with  $-\frac{\pi}{2} < \beta < 0$  with the positive  $x$ - axis. Further suppose that  $f(x, y_0) < 0$  and  $g(x, y_0) < 0$  for  $x$  slightly larger than  $x_0$ . Now

- (a) Prove that  $(x_0, y_0)$  is a stable equilibrium.
  - (b) Give an example of the above situation in which  $(x_0, y_0)$  is a stable focus.
  - (c) Give an example of the above situation in which  $(x_0, y_0)$  is a stable node.
7. The bursting phenomenon in §2.4.2 was discussed for  $k = -25$ ,  $\epsilon = 0.001$ . Try to reproduce it for other values of  $k$ , say for  $k = -40, -30, -20, -10$ . Do you also find bursting? If not, explain why.
  8. The bursting phenomenon in §2.4.2 was explained by using a bistability region in the fast Morris-Lecar system. Now from §2.1.2 we know that this fast system has another bistability region as well. Can you construct a model that has bursting due to the presence of this second bistability region?
  9. Produce Figure 2.8. Hint: start by computing a stable equilibrium for  $I_{app} = 0$  and  $v_3$  larger than the value for which BT1 is found. Then compute a branch of equilibria, detect a limit point and continue a branch of limit points. Check that it also contains a cusp point.
  10. In §2.2.2 the Generalized Hopf point GH1 was computed ( $v_3 = 2.0215262$ ,  $I_{app} = 255.90695$ ). Compute a limit point of cycles (LPC) nearby for  $v_3 = 5$ . Hint: Solution at  $I_{app} = 214.59443$ , the period is  $T = 20.6595$ .
  11. Compute a curve of LPC cycles, starting from the LPC found in the previous exercise. Does it end in GH1? Hint: Yes.

## Chapter 3

# A full two-parameter picture

Extending the results of the previous chapters, we now discuss a reasonably complete picture of the behaviour of the Morris-Lecar model in two free parameters. We recall that the Morris-Lecar equations are given in (1.13,1.14), with  $m_\infty$ ,  $w_\infty$ , and  $\tau$  given by (1.15), (1.16), and (1.17), respectively. The parameters different from  $I_{app}$  and  $v_3$  are those given in Table 2.2.  $I_{app}$  and  $v_3$  are varied in the tests. For simplicity we write  $I$  instead of  $I_{app}$ .

### 3.1 The global picture.

#### 3.1.1 Equilibria

In Figure 3.1, we subdivide the equilibrium bifurcation diagram in the most relevant parameter range for the Morris-Lecar model into different areas, depending on the number and stability of the equilibria.

In the white areas, there is only 1 equilibrium, and it is stable. In the pale gray area, the unique equilibrium is unstable.

In the other areas there are 3 equilibria, except on the borders: on the LP curves L and M there are exactly 2 equilibria, and in the CP point 2 there is only 1 equilibrium.

The dark gray area contains in each point 3 equilibria, of which 1 is stable and 2 are unstable. The 3 equilibria in the horizontally hatched area are all unstable.

Finally, the diagonally hatched area has 2 stable and 1 unstable equilibrium.

#### 3.1.2 Limit cycles

Figure 3.2 shows a qualitative diagram of all important limit cycle bifurcations that occur in the same parameter range for the Morris-Lecar model. Part of it corresponds to Figure 3.1, but we added the bifurcations of limit cycles (notably LPCs) and homoclinics as well as the codimension 2 points related to them.

In Figure 3.3 we present the phase diagrams for the areas as numbered in Figure 3.2. Phase diagrams for the relevant homoclinic bifurcations are shown in Figure 3.4.

Below the GH point 1, so for values  $v_3 < v_{3GH} = 2.02153$ , the rightmost Hopf point (curve B) consists of supercritical Hopf points: stable limit cycles are born and found at the left side of curve B. For  $v_3 > v_{3GH}$ , the Hopf points on curve B are subcritical: unstable periodic orbits are born and found at the right side of curve B. They then gain stability at the LPC curve C

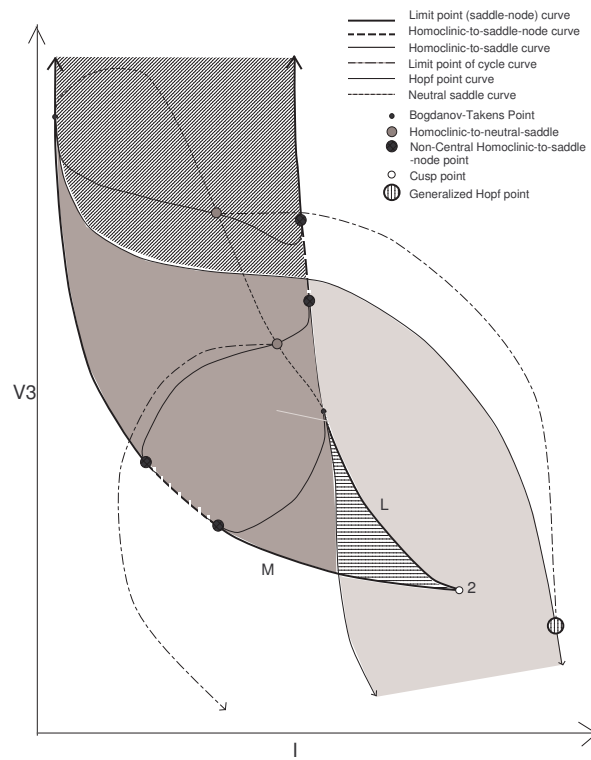


Figure 3.1: Qualitative bifurcation diagram in the biologically most relevant parameter range. Areas are coloured depending on the number and stability of the equilibria: white = 1 stable eq.; light gray = 1 unstable eq.; horizontal lines = 3 unstable eq.; diagonal lines = 2 unstable and 1 stable eq.; dark gray = 2 stable and 1 unstable eq.

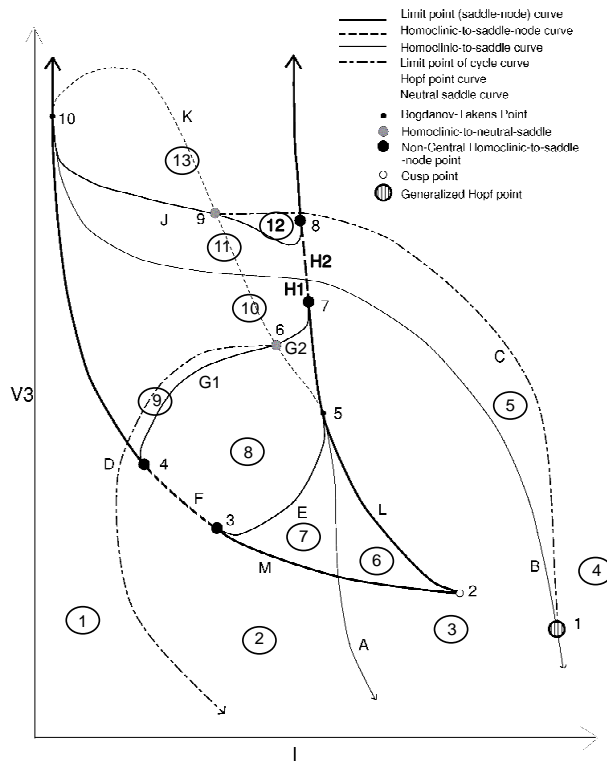


Figure 3.2: Qualitative bifurcation diagram in the biologically most relevant parameter range.  $v_3$ -values for the numbered points: 1 = 2.02153, 2 = 3.74191, 3  $\approx$  4.47, 4 = 4.48019, 5 = 9.67349, 6 = 10.88588, 7 = 12.42132, 8  $\approx$  9  $\approx$  17.25, 10 = 57.10678. The encircled numbers refer to phase diagrams for the different plot areas, shown in Figure 3.3.

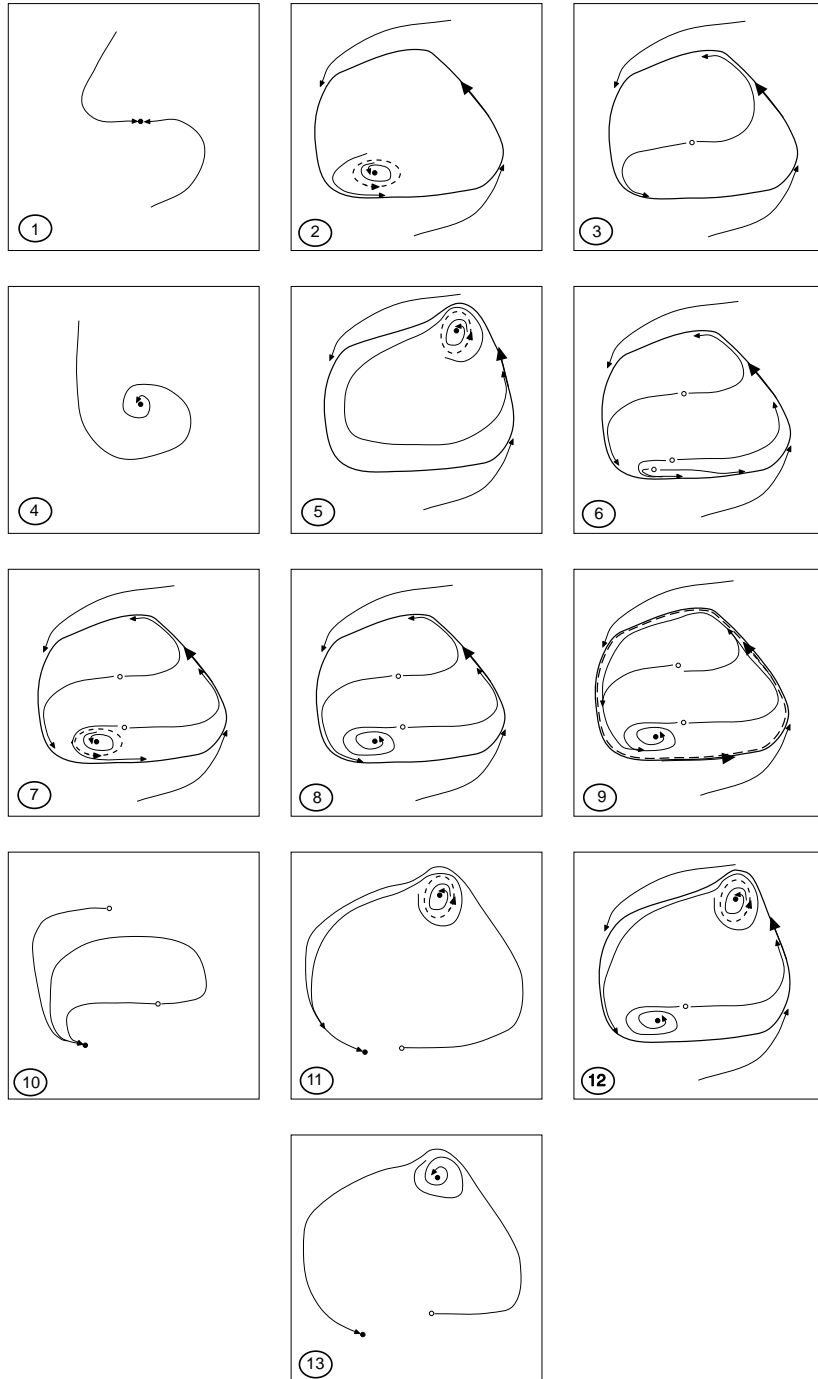


Figure 3.3: Phase diagrams for the areas as numbered in Figure 3.2.

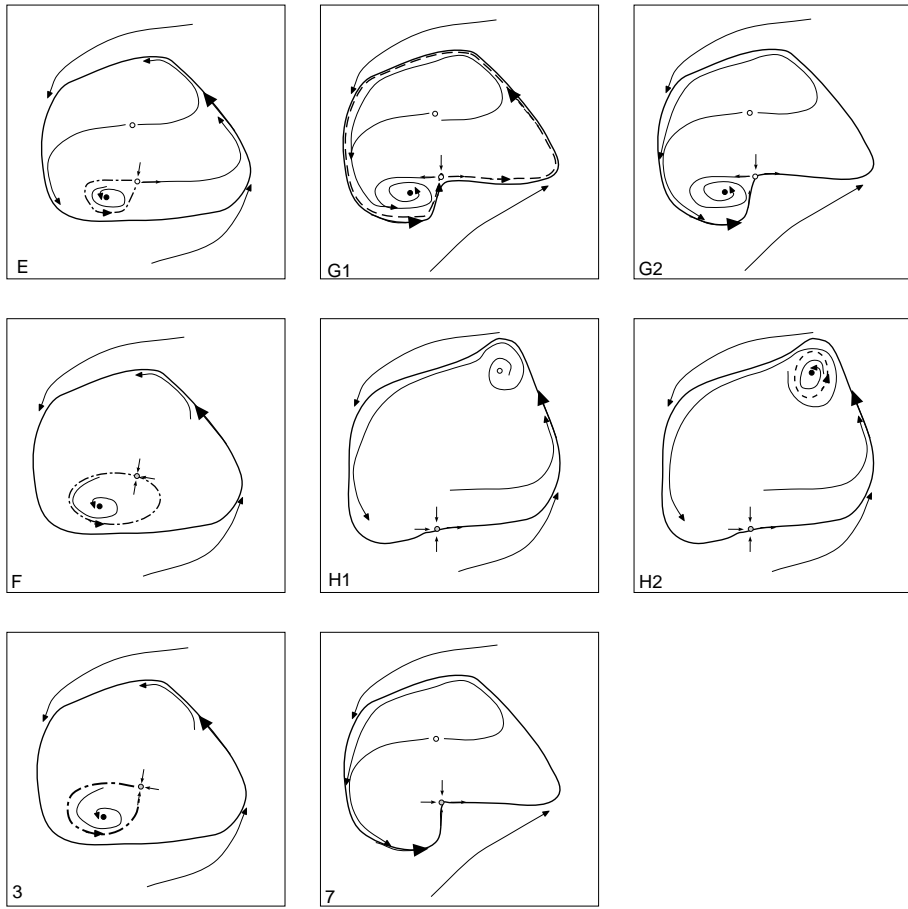


Figure 3.4: Phase diagrams for some homoclinic bifurcations. The letters and numbers in the lower left corners refer to the indications in Figure 3.2. The top 3 show homoclinic-to-hyperbolic-saddle bifurcations; the middle 3 show central homoclinic-to-saddle-node bifurcations; the bottom 2 show non-central homoclinic-to-saddle-node bifurcations.

and move to the left. We then have bistability of these stable periodic orbits and the stable equilibrium, with an unstable limit cycle between the two stable objects. When crossing the Hopf curve B, the stable equilibrium and unstable periodic orbits merge to become an unstable equilibrium but the stable orbit persists.

For fixed values of  $v_3$  below those of point 3 and decreasing values of  $I$  the stable periodic orbits again lose stability at the LPC curve D; they continue for increasing values of  $I$  as unstable periodic orbits and die at the subcritical Hopf curve A. The firing frequency of the neuron therefore remains in a bounded range.

From point 3 on, the limit cycles behave differently. Point 3 forms the transition between HHS and HSN orbits, and is called a Non-Central Homoclinic-to-Saddle-Node (NCH). It is located close to the value of  $v_{3HSN1} = 4.47$ . Point 4, which is the same type of point, is really close, at the value  $v_{3HSN2} = 4.48019$ . Between these two points, the unstable limit cycles that arise from the Hopf point on curve A never become stable, but instead end up in a HHS orbit on curve E. The stable limit cycles coming from higher  $I$ -values, lose stability at LPC curve D, and then converge to a HSN orbit on HSN curve F. So the stable limit cycles still cause bistability with the stable equilibrium. After they lose their stability, their period grows to infinity. Since this happens in the unstable regime of limit cycles, this does not influence the actual spiking of the neuron. The firing frequency range remains limited.

Above point 4 and below point 6, the stable limit cycles coming from the right, converge to a HHS bifurcation on curve G1, after losing stability at LPC curve D. This however doesn't change the general behavior.

Point 5 is a BT point, at  $v_{3BT} = 9.67349$ . For  $v_3 > v_{3BT}$ , the Hopf points on curve A no longer exist, and the only remaining limit cycles are the ones arising from the Hopf points on curve B. These are still born unstable, gaining stability at the LPC curve C and losing stability at LPC curve D. Thus, when we gradually increase input  $I$ , starting low, spiking will start at the limit point, and periods of the stable cycles are still limited in range.

We note that the classification by equilibrium bifurcation type at the onset of firing (Hopf or LP), as introduced by Rinzel and Ermentrout (1989), has no parallel classification in behavioral properties. The bifurcation point, the BT point, does not mark an important transition in firing ranges or onsets.

Point 6 is a NSS point, at  $v_{3HNS1} = 10.88588$  and the LPC curve D dies at that point. For higher values of  $v_3$  the stable limit cycles converge to the HHS orbits on curve G2. So we still get bistability, but firing frequencies can be arbitrarily low, i.e. the periods of the stable cycles can go to infinity.

The next important change happens at NCH point 7, at  $v_{3HSN3} = 12.42132$ . Here again a transition is made from HHS to HSN orbits. From this point on, there is no more bistability: the stable limit cycles converge to the HSN on curve H1 or H2.

Point 8 is another NCH point at  $v_{3HSN4}$ , but the  $v_3$ -value of this point, and of point 9, a NSS point, are extremely close together. They both lay somewhere around a  $v_3$ -value of 17.30. In the minuscule interval between points 8 and 9, there is again bistability: the stable limit cycles converge to the HHS orbit on curve J.

Point 10 is another BT-point, at  $v_3 = 57.10678$ . Between points 9 ( $v_3 = v_{3HNS2}$ ) and 10 there are only unstable limit cycles, and above point 10 there aren't any limit cycles left, so for these parameter ranges the neural model doesn't show any spiking behavior.

## 3.2 Exercises

### 1. Line $v_3 = 0$ . (below point 1 in Figure 3.2)

- (a) Compute by time integration a fixed point of the Morris-Lecar system for  $v_3 = 0$ ,  $I_{app} = 400$ .
- (b) Compute a curve of equilibria for  $v_3 = 0$  with  $I_{app}$  free. Which special points do you detect? Give the coordinates and the first Lyapunov numbers for two Hopf points on this curve. What do you conclude about the stability of the periodic orbits born at these Hopf points? At which side of the Hopf point do you expect to find the periodic orbits?
- (c) Compute a curve of periodic orbits starting at the first (supercritical) Hopf point, with  $I_{app}$  and the period free. Choose 50 mesh intervals, set `MaxStepsize=5`, `FunTolerance=1e-7`, `VarTolerance=1e-7`, `TestTolerance=1e-3`. Monitor  $I_{app}$ , the multipliers and the test function for LPC. What do you observe? Now repeat with `VarTolerance=1e-3`.

### 2. Line $v_3 = 15$ . (between points 7 and 8 in Figure 3.2)

- (a) Compute by time integration a fixed point of the Morris-Lecar system for  $v_3 = 15$ ,  $I_{app} = 400$ .
- (b) Compute a curve of equilibria for  $v_3 = 15$  with  $I_{app}$  free. Which special points do you detect? Give the coordinates of all special points and the first Lyapunov numbers for the Hopf point on this curve. What do you conclude about the stability of the periodic orbits born at the Hopf point? At which side of the Hopf point do you expect to find the periodic orbits? In which  $I_{app}$ -intervals do we have stable equilibria?
- (c) Compute a curve of periodic orbits starting from the Hopf point with  $I_{app}$  and the period as free parameters. Monitor  $I_{app}$ , the test function for LPC, the multipliers and the period. Present the computed orbits in  $(V, w)$ -space. Report the behaviour that you observe.

### 3. Line $v_3 = 11.5$ . (between points 6 and 7 in Figure 3.2)

- (a) Compute by time integration a fixed point of the Morris-Lecar system for  $v_3 = 11.5$ ,  $I_{app} = 400$ .
- (b) Compute a curve of equilibria for  $v_3 = 15$  with  $I_{app}$  free. Which special points do you detect? Give the coordinates of all special points and the first Lyapunov numbers for the Hopf point on this curve. What do you conclude about the stability of the periodic orbits born at the Hopf point? At which side of the Hopf point do you expect to find the periodic orbits? In which  $I_{app}$ -intervals do we have stable equilibria?

(c) Compute a curve of periodic orbits starting from the Hopf point with  $I_{app}$  and the period as free parameters. Monitor  $I_{app}$ , the test function for LPC, the multipliers and the period. Present the computed orbits in  $(V, w)$ -space. Report the behaviour that you observe.

4. **Line  $v3 = 3$ . (between points 1 and 2 in Figure 3.2)**
5. **Line  $v3 = 4$ . (between points 2 and 3 in Figure 3.2)**
6. **Line  $v3 = 7$ . (between points 4 and 5 in Figure 3.2)**
7. **Line  $v3 = 70$ . (above point 10 in Figure 3.2)**

## Chapter 4

# Cell cycle controls

The modern history of the study of the cell cycle goes back to 1976 when Paul Nurse (1949 -) identified the gene *cdc2* in yeast. This gene controls the cell cycle from G1-phase to S-phase and the transition from G2-phase to mitosis (cell division). In 2001 he received the Nobel Prize for Physiology or Medicine "for the discovery of cyclin and cyclin-dependent kinase, central molecules in the regulation of the cell cycle".

It was soon discovered that there exists a bewildering variety of cyclins and cyclin-dependent kinases. The information about proteins that control cell growth and cell division in eukaryotes (organisms whose genetic material is contained within a distinct nucleus) is enormous and the process of growth and division is very complex. An extra problem is that the details of the process vary from organism to organism and that many parameters are hard to determine by experimental methods. Experimental results are therefore usually obtained in a few special cases, like budding yeast (*Saccharomyces cerevisiae*), fission yeast (*Schizosaccharomyces pombe*) and frog egg cells.

However, the basic principles are by now reasonably well understood and present-day researchers work hard on building mathematical models, mainly in the form of systems of nonlinear ODEs. The present chapter is based on [3], Chapter 10 by J.J. Tyson and B. Novak. The basic ideas on modeling and bifurcation are already present in the "toy model", so for the bifurcation study we mainly concentrate on this situation to avoid a morass of details. But we mention also the more realistic model for budding yeast as given in [3]. Related papers also deal with fission yeast and frog egg cells.

### 4.1 The basic mechanisms

#### 4.1.1 The phases of the cell cycle

The process of cell growth and cell division is a continuous, cycling process that is usually divided into several stages in the order

$$\rightarrow M \rightarrow G1 \rightarrow S \rightarrow G2 \rightarrow M \rightarrow G1 \rightarrow,$$

traditionally portrayed in a schematic picture like Figure 4.1.

After a cell division phase (M for Mitosis), the daughter cells each have the same number and kind of chromosomes in their nuclei as the parent cell had. They then enter the first gap phase G1 during which they mainly grow and prepare for a possible further division.

Then, at a critical point (we call it "Start") they enter the start phase S during which they replicate their DNA, i.e. each chromosome copies itself and at the end of S phase consists of two identical sister chromatids which are held together by specific tethering proteins, called cohesins. This is followed by the second gap phase G2 during which the cell further grows and prepares for replication.

The M phase is the most complicated one and can further be subdivided into a metaphase ("meta" generically means "change of position" or "change of state" as in "metabolism") and an anaphase (the prefix "ana" can have several translations and here could be interpreted as "again" like in anabaptism). During the metaphase the so-called metaphase spindle or mitotic spindle is formed. This is a spindle-shaped mass of microtubules to whose opposite poles the sister chromatids are connected by microtubules. At another critical stage (we call it "Finish") the cell enters anaphase during which the cohesins are destroyed so that the sister chromatids can be segregated to opposite sides of the cell. Shortly thereafter, the cell itself divides and the two daughter cells are born in G1 stage, after which the cycle can start again.

This chromosome cycle of the cell normally runs in parallel with the growth cycle, whereby the other components of the cell (proteins, RNA, phospholipid bilayers, carbohydrates etc.) are also duplicated and partitioned between daughters. There are exceptions to this rule, such as oocytes (immature eggs in an ovary) which grow very large without dividing. The opposite phenomenon is found in embryos (fertilized eggs) which divide rapidly without growing. But these are temporary exceptions. In general, the long-term viability of a cell depends on balanced growth and division.

Typically, this is achieved in most cells by a size requirement for the Start transition. I.e., the process of chromosome replication in S phase will not start if the cell is not big enough. A second constraint is to hold off the Finish transition if DNA replication or chromosome alignment have not been performed properly.

#### 4.1.2 The regulatory mechanism

Cyclins are a family of proteins involved in the progression of cells through the cell cycle. They got their name from the fact that their concentration in the cell evolves periodically during the cell cycle. They are produced or degraded as needed in order to drive the cell through the different stages of the cell cycle.

To be active, a cyclin must form a complex with its partner cyclin-dependent kinase (Cdk), which activates the latter's protein kinase function. Such a complex is called a dimer, meaning simply that it consists of two substances (similarly, a trimer is a complex that consists of three substances). When the concentration of a cyclin in the cell is low, the cyclin detaches from the Cdk, inhibiting the enzyme's activity. It is generally assumed that the Cdk's are always present in abundance, so that the presence of the complexes is regulated by the availability of the cyclins. The role of the cyclin/Cdk dimers is to phosphorylate and hence deactivate proteins like the cohesins and enemy proteins of cyclins like Cdc20, cf. Figures 4.2 and 4.4.

The activity of the cyclin/Cdk dimers can be inhibited by phosphorylation, i.e. by binding with a phosphate group. As an additional layer of complexity, the Cyclin/Cdk dimers can be put out of commission by a third partner, a so-called CKI (cyclin-dependent kinase inhibitor). The synthesis and degradation of CKI's is also regulated by the cell cycle. Figure 4.3 gives an overall picture of the regulation of Cdk activity.

Higher eukaryotes contain many different cyclins and Cdks, which is one of the reasons why modeling of the cell cycle is rather difficult. However, lower eukaryotes such as yeast

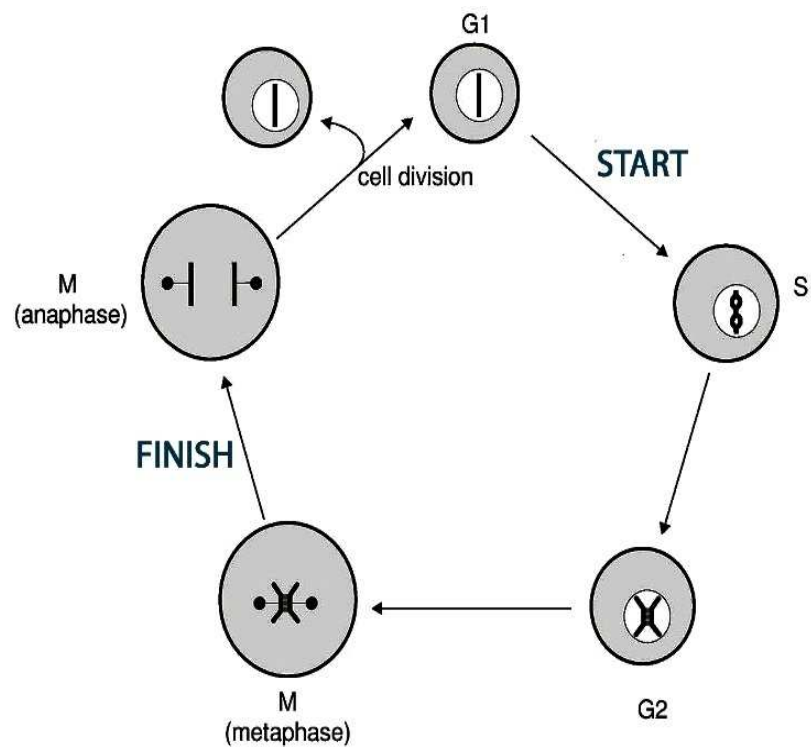


Figure 4.1: The cell cycle [12]. A newborn cell is initially in G1 phase. At start, the cell enters into S phase to replicate its DNA. After a gap (G2) phase, the cell enters into M phase, when the replicated chromosomes are aligned on the metaphase spindle. At Finish the cell is prepared to divide and shortly thereafter it divides to produce two daughter cells which are initially in G1 phase.

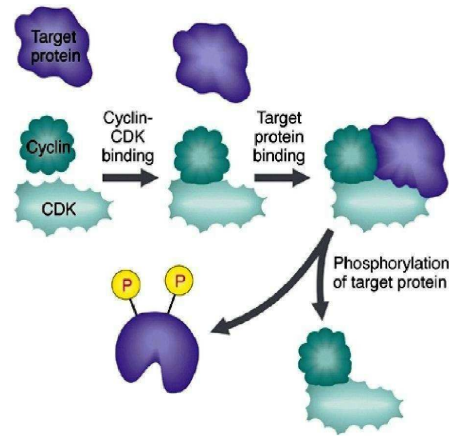


Figure 4.2: Cyclin-dependent kinase. Cyclin-dependent kinase (Cdk) requires a cyclin partner in order to be activated. It phosphorylates a target protein using ATP as the phosphate donor.

cells accomplish the same tasks with only one Cdk and 2-4 cyclins. This indicates that the different cyclin - Cdk pairs can more or less replace each other.

As described above, the cell cycle is usually divided into G1, S, G2 and M phases but it may be more convenient to subdivide it into the parts G1 and S-G2-M as proposed by K. Nasmyth [9]. The G1 phase is then correlated with low Cdk activity while the S-G2-M phase is correlated with high Cdk activity.

During G1, cyclin levels are low because cyclin mRNA synthesis is inhibited and cyclin protein is rapidly degraded. At Start, cyclin synthesis is induced and cyclin degradation is inhibited. The initial rise in Cdk activity initiates the replication of DNA (S phase) but a further increase is needed to drive the cell into the mitosis anaphase.

At Finish, a group of proteins, called the anaphase-promoting complex (APC) is activated. The APC attaches a "destruction label" to specific target proteins, which then are degraded by the cell's specific proteolytic (protein-killing) components. The APC contains, among other components, two proteins called Cdc20 and Cdh1. Activation of Cdc20 is needed for the degradation of the cohesins and for activation of Cdh1. Both Cdc20 and Cdh1 are needed to label cyclins for degradation, so that the control system can return to the low activity of cyclins in the G1 phase. The situation is complicated since cyclin/Cdk activates Cdc20 but inhibits Cdh1.

A simple theme runs through the morass of details. The transitions Start and Finish are irreversible and related to the antagonistic relationship between the central components of the cell cycle machinery. The APC extinguishes Cdk activity by destroying cyclins, while cyclin/Cdk dimers inhibit APC by phosphorylating Cdh1. This leads, roughly speaking, to two stable steady states of the systems: a G1 state with high Cdh1/APC activity and low cyclin/Cdk activity, and a S-G2-M state with high cyclin/Cdk activity and low Cdh1/APC activity.

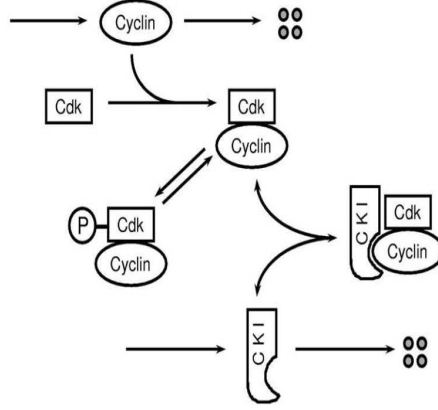


Figure 4.3: Regulation of Cyclin- dependent kinase activity [12]. Cyclin- dependent kinase (Cdk) can be activated by cyclin subunits, and deactivated by phosphorylation of the Cdk subunit or by binding to inhibitors.

#### 4.1.3 Example: the budding yeast equations.

As an example we present the budding yeast equations for a fixed cell mass  $m$ , as given by Tyson and Novák [3]:

$$\begin{aligned}
\frac{d[CycB]_T}{dt} &= k_1 - (k'_2 + k''_2[Cdh1] + k'''_2[Cdc20]_A)[CycB]_T, \\
\frac{d[Cdh1]}{dt} &= \frac{(k'_3 + k''_3[Cdc20]_A)(1 - [Cdh1])}{J_3 + 1 - [Cdh1]} - \frac{(k_4 m [CycB] + k'_4 [SK])[Cdh1]}{J_4 + [Cdh1]}, \\
\frac{d[Cdc20]_T}{dt} &= k'_5 + k''_5 \frac{(m [CycB])^n}{J_5^n + (m [CycB])^n} - k_6 [Cdc20]_T, \\
\frac{d[Cdc20]_A}{dt} &= \frac{k_7 [IEP]([Cdc20]_T - [Cdc20]_A)}{J_7 + [Cdc20]_T - [Cdc20]_A} - \frac{k_8 [Mad][Cdc20]_A}{J_8 + [Cdc20]_A} - k_6 [Cdc20]_A, \\
\frac{d[IEP]}{dt} &= k_9 m [CycB] (1 - [IEP]) - k_{10} [IEP], \\
\frac{d[CKI]_T}{dt} &= k_{11} - (k'_{12} + k''_{12}[SK] + k'''_{12}[CycB])[CKI]_T, \\
\frac{d[SK]}{dt} &= k'_{13} + k''_{13}[TF] - k_{14}[SK], \\
\frac{d[TF]}{dt} &= \frac{(k'_{15} m + k''_{15}[SK])(1 - [TF])}{J_{15} + 1 - [TF]} - \frac{(k'_{16} + k''_{16} m [CycB])[TF]}{J_{16} + [TF]},
\end{aligned} \tag{4.1}$$

where

$$[CycB] = [CycB]_T - [Trimer].$$

In building this model it is assumed (quasi-steady state hypothesis!) that  $CKI/CycB/Cdk$  trimers are always in equilibrium with  $CKI$  monomers and  $CycB/Cdk$  dimers. To be precise, the reactions



lead to the equation

$$\frac{d[Trimer]}{dt} = k^- [CKI][CycB/Cdk] - k^+ [Trimer],$$

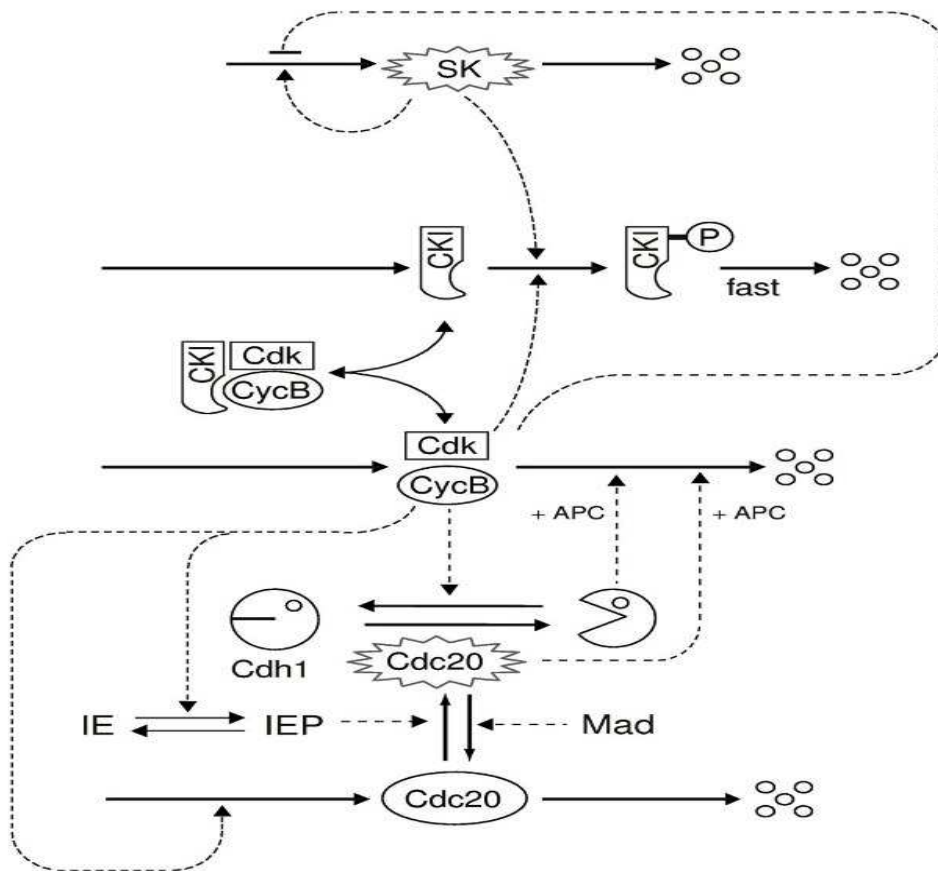


Figure 4.4: The basic cell cycle engine in eukaryotic cells [12]. Dynamical properties of this mechanism are determined by sets of kinetic equations in the form of differential equations.

Table 4.1: Fixed parameters in (4.1)

Parameter	Value	Parameter	Value	Parameter	Value
$k_1$	0.04	$k_9$	0.1	$J_3$	0.04
$k'_2$	0.04	$k_{10}$	0.02	$J_4$	0.04
$k''_2$	1	$k_{11}$	1	$J_5$	0.3
$k'''_2$	1	$k'_{12}$	0.2	$J_7$	$10^{-3}$
$k'_3$	1	$k''_{12}$	50	$J_8$	$10^{-3}$
$k''_3$	10	$k'''_{12}$	100	$J_{15}$	0.01
$k'_4$	2	$k'_{13}$	0	$J_{16}$	0.01
$k_4$	35	$k''_{13}$	1	$n$	4
$k'_5$	0.005	$k_{14}$	1	$[Mad]$	1
$k''_5$	0.2	$k'_{15}$	1.5	$K_{eq}$	1000
$k_6$	0.1	$k''_{15}$	0.05		
$k_7$	1	$k'_{16}$	1		
$k_8$	0.5	$k''_{16}$	3		

and we assume that the reactions in (4.2) are so fast that equilibrium is attained instantaneously, i.e.

$$[Trimer] = K_{eq}[CycB][CKI] = K_{eq}([CycB]_T - [Trimer])([CKI]_T - [Trimer]),$$

where  $K_{eq} = \frac{k^-}{k^+}$ . Hence

$$[Trimer] = \frac{2[CycB]_T[CKI]_T}{\Sigma + \sqrt{\Sigma^2 - 4[CycB]_T[CKI]_T}},$$

where

$$\Sigma = K_{eq}^{-1} + [CycB]_T + [CKI]_T.$$

The form of this system of equations can be related to the regulatory path in Figure 4.4. For a fuller discussion we refer to [3]. However, it is important to know that  $[CycB]_T$  is a measure for the concentration of cyclins while  $[Cdh1]$  is a measure for the concentration of APC's. Typically,  $[CycB]_T$  is low and  $[Cdh1]$  is high during G1 phase and vice versa during S-G2-M phase.

The values of the fixed parameters in (4.1) are given in Table 4.1.

For a growing cell, one equation is added:

$$\frac{dm}{dt} = \mu m \left(1 - \frac{m}{m_*}\right). \quad (4.3)$$

The rationale of this assumption is that cells grow at a constant relative rate  $\mu$  when they are small and there is some intrinsic threshold  $m_*$  above which they cannot grow. This is, of course, a form of the logistic equation. However, in the applications it is always assumed that the cell divides long before this threshold is reached. Therefore, the precise value of  $m_*$  is irrelevant and the factor  $(1 - \frac{m}{m_*})$  is sometimes dropped.

## 4.2 The toy model of Tyson and Novak

### 4.2.1 The model with constant Cdh1/APC activator

In a toy setting, Tyson and Novak [3], §10.3.1, propose the following nondimensionalised model for the cell cycle

$$\frac{dX}{dt} = k_1 - (k'_2 + k''_2 Y)X, \quad (4.4)$$

$$\frac{dY}{dt} = \frac{(k'_3 + k''_3 A)(1 - Y)}{J_3 + 1 - Y} - \frac{k_4 m XY}{J_4 + Y}. \quad (4.5)$$

Here  $X$  and  $Y$  are the concentrations of cyclin/Cdk dimers and active Cdh1/APC complexes, respectively. We assume that APC cores are abundantly available and that the total Cdh1 concentration is constant, so that it can be scaled to 1. Therefore  $Y$  is always between 0 and 1.

In (4.4) and (4.5),  $m$  and  $A$  are the main bifurcation variables.  $m$  is a measure of the volume of the cell and  $A$  represents the concentration of a protein that can activate Cdh1 at Finish.

The equation (4.4) can be interpreted as follows:

- $k_1$  is the (constant) production rate of cyclins; these combine rapidly with the Cdk's which are available in abundance.

- $k'_2$  is the (constant) degradation rate of the Cdk/cyclin complexes.

- $k''_2$  is the constant in the law of mass action that models the extinction of the Cdk/cyclin activity by active Cdh1/APC complexes.

The right-hand side of (4.5) consists of two terms. The first term

$$\frac{(k'_3 + k''_3 A)(1 - Y)}{J_3 + 1 - Y}$$

is not dependent on  $X$ . It represents a Michaelis-Menten equation for the dephosphorylation reaction of Cdh1. So  $J_3$  is a Michaelis-Menten constant and  $(k'_3 + k''_3 A)$  is the maximal rate of dephosphorylation ( $J_3$  is much smaller than 1.) The interpretation is that  $k'_3$  is the maximal rate for  $A = 0$  (no protein to activate Cdh1 is available) and that the maximal production rate grows linearly with  $A$ .

The second term

$$-\frac{k_4 m XY}{J_4 + Y}$$

represents a Michaelis-Menten type equation for the phosphorylation reaction of Cdh1 where  $J_4$  is another Michaelis-Menten constant and  $k_4 m X$  is a maximal production rate. The rationale behind this is that the cyclin/Cdk dimers are assembled in the cytoplasm (cell plasma) and then move into the nucleus of the cell, so that the total amount of cyclin/Cdk dimers in the nucleus is, in fact, proportional to the cell mass  $m$ .

The fixed values of the parameters other than  $m$ ,  $A$  (rate constants and Michaelis-Menten constants) are given in Table 4.2.

In a computational study of these equations we start with parameter values  $A = 0$ ,  $m = 0.3$ , and perform time integration, starting (rather arbitrarily) with  $X = 0.05$ ,  $Y = 0.9$ . The computed orbit converges fast to the point  $X = 0.0394$ ,  $Y = 0.9735$ , which in the cell cycle interpretation corresponds to G1-phase (cyclins  $X$  low, active Cdh1/APC  $Y$  high).

Parameter	Value
$k_1$	0.04/min
$k_2'$	0.04/min
$k_2''$	1/min
$k_3'$	1/min
$k_3''$	10/min
$k_4$	35/min
$J_3$	0.04
$J_4$	0.04

Table 4.2: Fixed rate constants and Michaelis-Menten constants in (4.4) and (4.5).

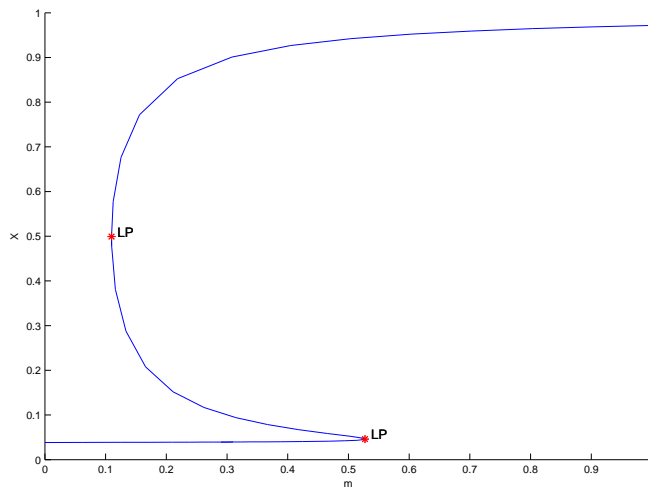


Figure 4.5: Equilibria of (4.4), (4.5) for  $A = 0$ .

We select the equilibrium, compute a curve of equilibria with  $m$  free, and plot the result in  $(m, X)$ -space, see Figure 4.5. We obtain a typical S-shaped curve with two limit points, namely for  $m = 0.527319$  with  $X = 0.046085$ ,  $Y = 0.827956$  and for  $m = 0.109714$  with  $X = 0.499163$ ,  $Y = 0.040134$ .

Both the lower part of the curve (low values of  $X$ , corresponding to G1 phase) and the upper part (high values of  $X$ , corresponding to S-G2-M phase) are stable. The intermediate part between the two LP-points is unstable.

To understand the interplay between the parameters  $m, A$  we compute the bifurcation diagram in  $(m, A)$ -space, see Figure 4.6. This diagram is simple: the thick solid line and the thick dashed line are both limit point curves; the thin dotted line is a curve of equilibrium points for fixed  $A = 0.1$ . The G1 state is stable in all points above the solid line, the S-G2-M state is stable below the thick dashed line. Of course, only points with  $m > 0, A \geq 0$  are meaningful in the model.

Now, if we are in the region where G1 is stable and  $m$  increases, then inevitably we cross the thick solid line at some point, the G1 state loses stability and the system must turn to the (now stable) S-G2-M state. Conversely, if we are in a region where S-G2-M is stable and  $A$  increases sufficiently, then at some point we cross the thick dashed line, the S-G2-M state loses stability and the system must jump to the (now stable) G1 state. So it is understandable

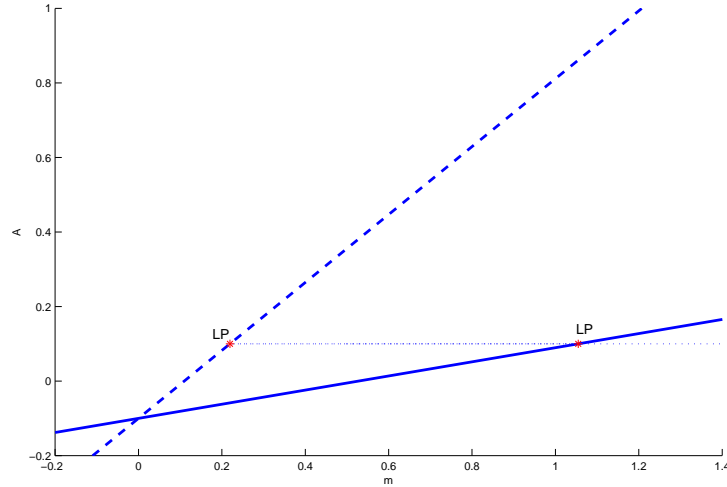


Figure 4.6: Two curves of limit points in the model (4.4), (4.5).

that the cycle can be controlled by alternate increases of  $m$  and  $A$ .

#### 4.2.2 A dynamic Cdh1/APC activator

To improve the model (4.4)-(4.5) we must add a dynamic equation for  $A$ , i.e., the activator of Cdh1/APC at Finish. It must explain why  $A$  increases abruptly at Finish and decreases again rapidly in G1 phase. In reality it is a phosphatase Cdc14 that removes from Cdh1 the inhibitory phosphate groups placed there by the cyclin/Cdk (cf. the form of (4.5)). In fact, Cdc14 itself is activated indirectly: if the concentration of cyclin/Cdk is high enough, then it turns on Cdc20/APC which destroys an inhibitor for Cdc14.

To obtain a simple model, we just remember that if cyclin/Cdk is high enough in the nucleus of the cell, i.e., if  $mX$  is sufficiently large, then Cdc14 is produced. This leads to the following equation:

$$\frac{dA}{dt} = k'_5 + k''_5 \frac{(mX)^n}{J_5^n + (mX)^n} - k_6 A, \quad (4.6)$$

We note that  $\frac{(mX)^n}{J_5^n + (mX)^n}$  is a sigmoid function of  $mX$ : it is close to zero for values of  $mX$  that are much smaller than  $J_5$  and close to 1 for values of  $mX$  much larger than  $J_5$ . By increasing the Hill exponent  $n$  we increase the steepness of the sigmoid curve at the point where  $mX = J_5$ .

In (4.6) we have further assumed that  $A$  is produced at constant absolute rate  $k'_5$  and degraded at constant relative rate  $k_6$ . The values of the new rate constants, threshold constant and Hill exponent are given in Table 4.3. We note that with these values the rest state of  $A$  (when  $X$  is zero) is  $\frac{k'_5}{k_6} = 0.05$  is very low. Furthermore, if the system is in state G1 and  $m$  increases, then the system loses stability through the limit point bifurcation before the threshold for  $mX$  to activate  $A$ , i.e. the value 0.3 of  $J_5$ , is attained, see Figure 4.5.

We also note that a negative feedback loop is involved: the cyclin/Cdk ( $X$ ) turns on the activator ( $A$ ) which activates Cdh1 ( $Y$ ) which turns off the cyclin/Cdk.

Parameter	Value
$k'_5$	0.005/min
$k''_5$	0.2/min
$k_6$	0.1/min
$J_5$	0.3
$n$	4

Table 4.3: Fixed rate constants, Michaelis-Menten constant and Hill exponent in (4.6).

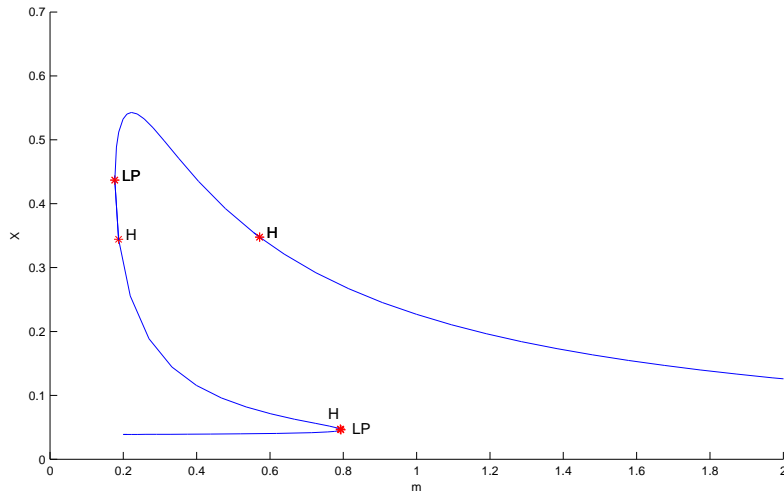


Figure 4.7: Equilibrium bifurcation diagram of (4.4), (4.5),(4.6) .

The basic equilibrium bifurcation diagram of (4.4), (4.5), (4.6) is given in Figure 4.7. The bottom part of the equilibrium curve represents stable equilibria (essentially corresponding to G1 state); the stability is lost at an LP point. The two further points denoted by H (one of which is very close to the LP point) are, in fact, neutral saddles and do not change the stability. Stability is regained at the second LP point ( $X$  near 0.43) and lost again at a subcritical Hopf point (H, where  $X$  is near 0.35 and  $m$  near 0.6). The unstable periodic orbits born at the Hopf point die at a homoclinic-to-saddle orbit and are not relevant to the modeling.

By time simulation for  $m = 0.9$  we can get a rough idea of the behaviour of (4.4), (4.5),(4.6) for values of  $m$  beyond the stability region. We find that the orbits rapidly converge to a stable periodic orbit with period near 70; see Figures 4.8, 4.9. One should note that most of time  $X$  is low (near 0.03) and  $Y$  is high (above 0.9); during this time  $A$  slowly decreases to a bottom value. These longer periods are interrupted by an upsurge of  $A$  and a rapid but short-lived reversal of the values of  $X$  and  $Y$ ; we note that the decrease of  $Y$  precedes the upsurge of  $X$ .

This behaviour is crucial for the interpretation of the model: increasing  $m$  provokes a decline of  $Y$  (notice the high value of  $k_4$ ), which in turn provokes an increase of  $X$ . The combined effect of increasing both  $m$  and  $X$  leads to a fast increase of  $A$ . This upsurge constitutes the Finish transition in the cell cycle; now the cell divides and the daughter cells are formed with lower values of  $m$ , and so they will be in the G1 phase.

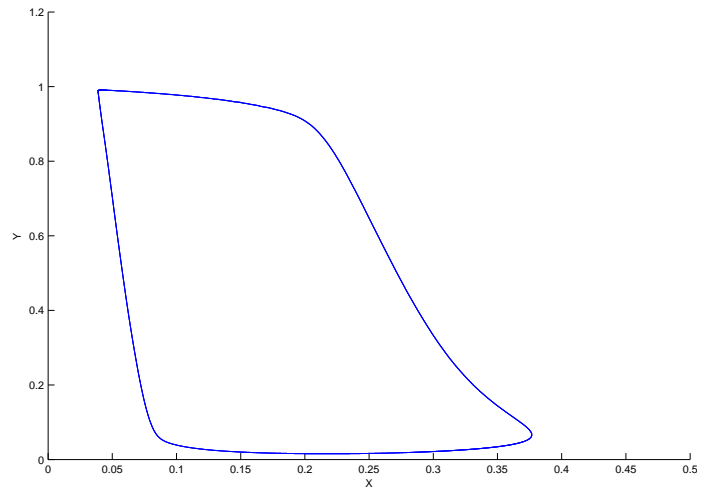


Figure 4.8: Simulation of (4.4), (4.5),(4.6) for  $m = 0.9$  in  $(X, Y)$  -space.

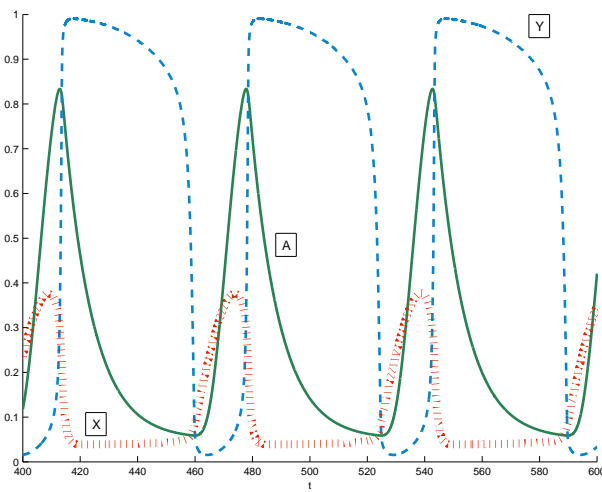


Figure 4.9: Simulation of (4.4), (4.5),(4.6) for  $m = 0.9$  (all variables versus  $t$ ).

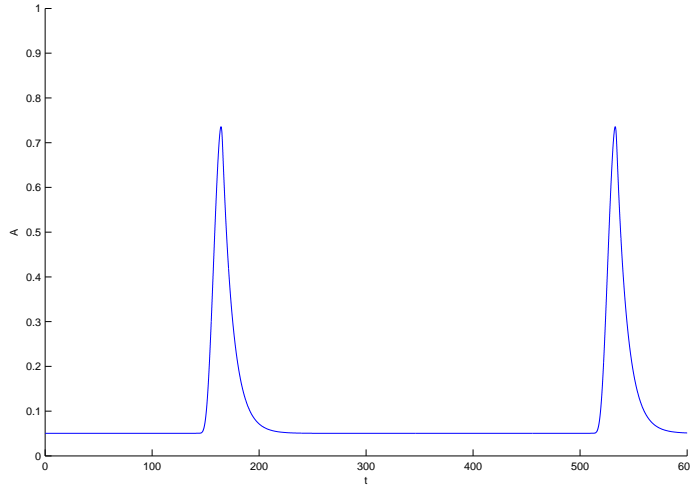


Figure 4.10: Simulation of (4.4), (4.5),(4.6) for  $m = 0.7927$  in  $(t, A)$  -space.

### 4.3 Orbits homoclinic to saddle-node

If we repeat the previous experiment for lower values of  $m$ , but still larger than the value  $m = 0.7926331$  at the limit point in Figure 4.7, then we get similar pictures but with gradually increasing periods. If we start with the state and parameter values of the limit point, but increase  $m$  slightly to 0.7927, then in  $(t, A)$  -space we obtain the picture in Figure 4.10.

To get a better understanding of what is happening, we can perform a continuation of periodic orbits, starting from the orbit computed in §4.2.2 for  $m = 0.9$  and represented in Figures 4.8, 4.9. We see that the period increases limitless if  $m$  tends to the limit point value  $m = 0.7926331$ . For example, for  $m = 0.79304204$  the period is 207.87322. In Figure 4.11 we present the period  $T$  as a function of  $m$ . The periodic orbit tends to an orbit homoclinic to saddle-node, the saddle-node being the lower limit point in Figure 4.7.

During G1 phase of the cell cycle  $m$  increases steadily along the lower equilibrium curve in Figure 4.7. The equilibrium loses stability when  $m$  gets larger than the limit point value and the dynamics of the system is then taken over by the homoclinic orbit which brings it to the Finish transition.

So the presence of an orbit homoclinic to saddle-node is crucial in this scenario. But how persistent is the presence of such an orbit? We can get an idea by the continuation of the orbit in two parameters. In the case where the free parameters are  $k_4$  and  $m$  we find that the orbit dies at a non-central homoclinic to saddle-node orbit for  $k_4 = 21.294025$ ,  $m = 1.3309616$ . In Figure 4.12 we present a picture in  $(X, Y)$ - space of this continuation; the inner orbit is the non-central homoclinic to saddle-node orbit (NCH).

### 4.4 The cell cycle as a slow-fast system: insensitivity to the initial values

To model cell division we must consider the cell mass  $m$  as a dynamic variable. As in the full budding yeast model a reasonable candidate for this behaviour is the next equation:

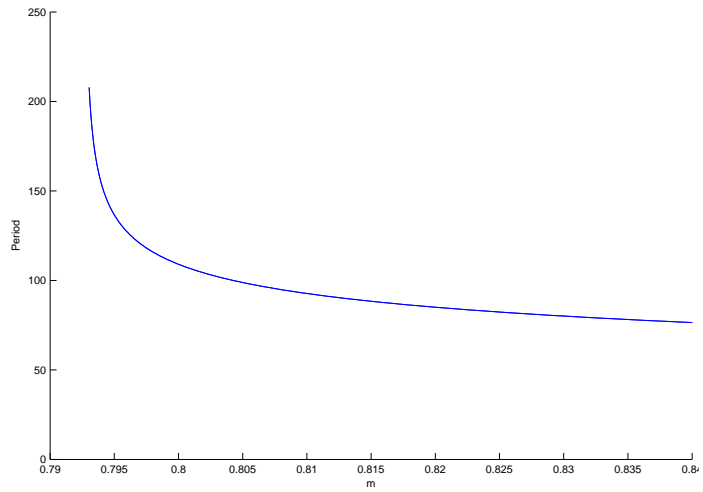


Figure 4.11: Periods of periodic orbits of (4.4), (4.5),(4.6) tending to an orbit homoclinic to saddle-node.

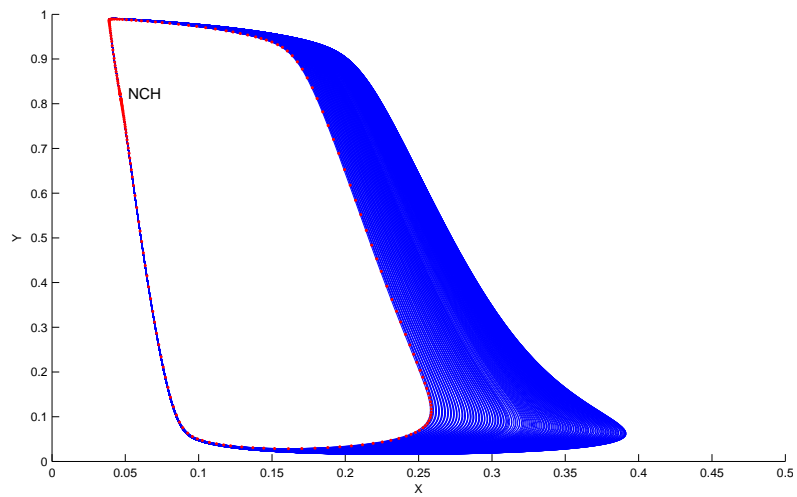


Figure 4.12: A curve of HSN orbits of (4.4), (4.5),(4.6) tending to a non-central homoclinic to saddle-node orbit.

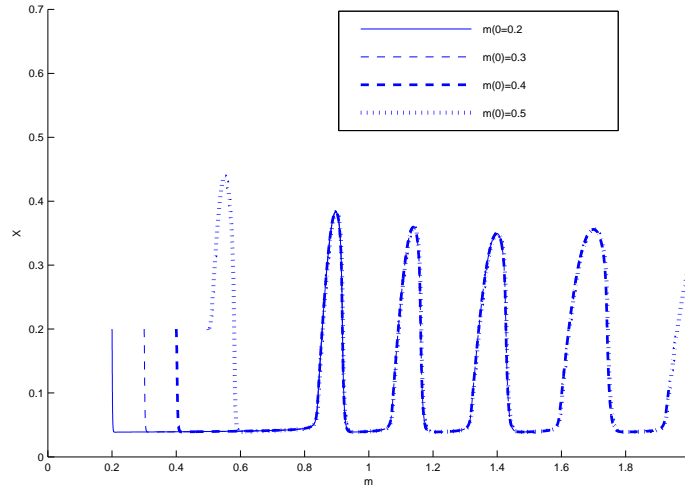


Figure 4.13: Four orbits of (4.4-4.7).

$$\frac{dm}{dt} = \mu m \left(1 - \frac{m}{m_*}\right). \quad (4.7)$$

In this equation  $\mu$  is the normal growth rate of the cell when  $m$  is small.  $m_*$  is a threshold above which  $m$  cannot grow for physical reasons (its value does not matter, if at least it is not too low).

We note that (4.7) is, again, a logistic equation and can be solved analytically. In fact, we have for starting values  $m(0) = m_0 \in ]0, m_*[$  that

$$m(t) = \frac{m_0 m_*}{m_0 + (m_* - m_0)e^{-\mu t}}, \quad t \in [0, \infty[. \quad (4.8)$$

In Figure 4.13 we present 4 orbits of (4.4-4.7) for the same time interval 350, the same parameter values as in Tables 4.2 and 4.3,  $\mu = 0.005$  and  $m_* = 10$ . They all start from an initial point with  $X(0) = Y(0) = A(0) = 0.2$ . However,  $m(0)$  takes the values 0.2, 0.3, 0.4, 0.5, respectively.

Two interesting things are to be observed. First, the four orbits (and many others that we can draw from different initial values for  $X, Y, A, m$ ) may differ initially, but they then all converge to practically the same orbit. Second, this "universal" orbit nearly coincides with the equilibrium branch in Figure 4.7 for low values of  $X$  as long as  $m$  is smaller than the lower limit point value  $m_{LP}$  of (4.4-4.6).

Here we have an example of extreme insensitivity to initial conditions. It is not hard to figure out why this happens. For values  $m$  below  $m_{LP}$  the system (4.4-4.6) has a stable equilibrium at the bottom branch of Figure 4.7. Since  $m$  increases slowly, the system (4.4-4.7) behaves locally as if  $m$  were constant, i.e. the orbit converges to the equilibrium of (4.4-4.6). Of course, this no longer holds if  $m > m_{LP}$  but by then the different orbits are so close together that they continue to behave as one orbit. This type of behaviour is sometimes called the funneling effect.

This behaviour makes biological sense since it ensures that the fate of a cell is eventually the same, whatever its origin was.

## 4.5 The cell cycle as a boundary value problem

Let us assume that the cell cycle starts at time  $t = 0$  when a newborn cell has mass  $m(0) = m_0$  and that the cell divides at time  $T$  when a new cell with mass  $m_0 = \nu m(T)$ ,  $0 < \nu < 1$  is born. We note that in cases like budding yeast  $\nu \ll 0.5$  since the cell does not divide in equal parts; it is rather a bud that detaches itself from the mother cell and starts an independent life.

The cell cycle can then be modeled as an orbit  $(X(t), Y(t), A(t), m(t))$  with the property that  $X(T) = X(0)$ ,  $Y(T) = Y(0)$ ,  $A(T) = A(0)$ ,  $\nu m(T) = m(0)$  with a cell cycle duration  $T$ . By (4.8) there is a relation between  $m_0$ ,  $\mu T$  and  $\nu$ , namely

$$\nu m_* = m_0 + (m_* - m_0)e^{-\mu T}. \quad (4.9)$$

Of course, this does not fully determine the cell cycle. We must decide at which point the cell is supposed to divide and this decision can be based on a value of  $X, Y, A, m$  or a combination of these values. Fortunately, we have seen in §4.4 that the fate of a cell is unique after passing the threshold point where  $m = m_{LP}$ ; so it does not really matter which variable we consider.

Based on Figure 4.13 we can propose that division take place for  $m = 0.096$ . If we further assume that  $\nu = 0.1$  and  $\mu = 0.005$ , then from 4.9 we find that

$$T = T_{CC} = -\frac{1}{0.005} \ln \frac{1 - 0.096}{10 - 0.096} \approx 478.7729269064402.$$

The boundary value is now determined completely by the condition that  $m(0) = 0.096$ ,  $T = T_{CC}$ ,  $X(T) = X(0)$ ,  $Y(T) = Y(0)$ ,  $A(T) = A(0)$ . Typically, such a boundary value problem must be solved by a discretization as the solution to a large, sparse system of nonlinear equations. However, in this case we can do better by noting that the solution is the fixed point of the map

$$M : \mathbb{R}^3 \rightarrow \mathbb{R}^3$$

where the initial point of the map is a vector  $(X(0), Y(0), A(0))^T$  and the map is obtained by adding to this vector the value  $m(0) = 0.096$ , integrating (4.4-4.7) over the time interval 478.7729269064402, and removing the fourth component from the output vector.

Starting from the initial vector

$$x_0 = \begin{bmatrix} 0.2 \\ 0.2 \\ 0.2 \end{bmatrix}$$

we find

$$x_1 = M(x_0) = \begin{bmatrix} 0.039005785357016 \\ 0.984241868798850 \\ 0.345641334333945 \end{bmatrix},$$

$$x_2 = M(x_1) = \begin{bmatrix} 0.039005776185400 \\ 0.984241137550836 \\ 0.345647210875336 \end{bmatrix},$$

$$x_3 = M(x_2) = \begin{bmatrix} 0.039005743113372 \\ 0.984195458286948 \\ 0.345647338829453 \end{bmatrix}.$$

Comparing these vectors we find that

$$\begin{aligned}\|x_0 - x_1\| &= 1.186870609709495, \\ \|x_1 - x_2\| &= 5.921870185849841e - 006, \\ \|x_2 - x_3\| &= 4.567945506925697e - 005.\end{aligned}$$

Hence a fixed point iteration converges extremely fast to the attainable accuracy.

## 4.6 Exercises

1. Draw a phase plane portrait of the nullclines of (4.4) and (4.5) for the parameter values in Table 4.2 with  $A = 0$  and  $m = 0.3$ . How many equilibria do you find? Which ones are stable, respectively unstable? What is the interpretation of these equilibria in the cell cycle model?
2. Same exercise as the previous but with  $m = 0.6$ . What is the main difference? Is there a reason to guess that there was a bifurcation for  $m$  between 0.3 and 0.6?
3. Consider the individual terms in (4.1). Can you relate them to the regulatory path in Figure 4.4?
4. Figure 4.6 looks unusual because in generic two-parameter systems limit point curves do not cross transversally. We expect that they meet in cusp points. But do they really cross in Figure 4.6? Check by graphical projection on the  $X$ - and  $Y$ - axes whether they really intersect (and not just their projections on  $(m, A)$ - space intersect.)
5. Check the values of  $X$  and  $Y$  along the limit point curves in Figure 4.6. Do you remark something unusual? And can you explain it?
6. In the Hopf point in Figure 4.7 (recall that two of the points marked as 'H' are in fact neutral saddle equilibria with two zero-sum real eigenvalues) unstable periodic orbits are born. For decreasing  $m$  they die at an orbit homoclinic to saddle. For which value of  $m$  is the homoclinic-to-saddle orbit found (find it by continuation)?
7. It is well known that a fixed point of a map is asymptotically stable if all the multipliers, i.e. the eigenvalues of the Jacobian matrix of the map, have modulus less than 1. Compute numerically (i.e. by finite differences) the Jacobian matrix of the map considered in §4.5 and find its eigenvalues. Check that they all have absolute values less than 1.
8. How do the results in §4.5 depend on the value  $m_*$  (which was chosen rather arbitrarily, after all)? To check your answer, perform the computations in §4.5 for another value of  $m_*$ , say  $m_* = 20$ . Discuss also what happens for  $m_* \rightarrow \infty$ .
9. How do the results in §4.5 depend on the value  $\mu$  (which was chosen rather arbitrarily, after all)? To check your answer, perform the computations in §4.5 for other values of  $\mu$ , say  $\mu = 0.01, 0.05, 0.1$ . In particular, consider the fixed point iteration. Does it also converge in one step?
10. Study the budding yeast model as given in (4.1) and (4.3). Do you find results similar to those in §4.4 and §4.5? Consider also the stability of the fixed point as in the previous exercise for the toy model.

# Bibliography

- [1] K. Cole, *A Quantitative Description of Membrane Current and its Application to Conductance and Excitation in Nerve*, University of California Press, Berkeley.
- [2] J. Emsley, *The Elements of Murder. A History of Poison*. Oxford University Press, Oxford 2005.
- [3] C.P.Fall, E.S.Marland, J.M.Wagner and J.J.Tyson, *Computational Cell Biology*, Springer 2002.
- [4] A. Hodgkin and A. Huxley, *Action potentials recorded from inside a nerve fibre*, J. Physiol. 144(1939) 710-711.
- [5] A. Hodgkin and A. Huxley, *A quantitative description of membrane current and its application to conduction and excitation in nerve*, J. Physiol. 117 (1952) 500-544.
- [6] Yuri A. Kuznetsov, *Elements of Applied Bifurcation Theory*, Applied Mathematical Sciences 112 (3rd edition),Springer 2004.
- [7] D. McCormick, *Membrane potential and action potential*, in: *Fundamental Neuroscience*, eds. M.J.Zigmond, F.E.Bloom, S.C.Landis, J.L. Roberts and L.R. Squire, Academic Press, New York 1999.
- [8] C. Morris and H. Lecar *Voltage oscillations in the barnacle giant muscle fiber*, Biophys. J. 35 (1981) 193-213.
- [9] K. Nasmyth *At the heart of the budding yeast cycle*, Trends Genet. 12 (1996) 405-412.
- [10] D. Terman *Chaotic spikes arising from a model of bursting in excitable membranes*, SIAM J. Appl. Math. 51 (1991) 1418-1450.
- [11] D. Terman *The transition from bursting to continuous spiking in excitable membrane models*, J. Nonlinear Sci. 2 (1992) 135-182.
- [12] Ch.P.Fall, E.S. Marland, J.M. Wagner and J.J. Tyson *Computational Cell Biology* Springer (2002) Chapter 10 :261-284.